


July 2022

A Protein-Based Therapeutic Combination for the Treatment of Hard-to-Heal Wounds

Graham L. Strauss
University of South Florida

Follow this and additional works at: <https://digitalcommons.usf.edu/etd>

 Part of the [Biomedical Engineering and Bioengineering Commons](#), [Molecular Biology Commons](#), and the [Other Chemistry Commons](#)

Scholar Commons Citation

Strauss, Graham L., "A Protein-Based Therapeutic Combination for the Treatment of Hard-to-Heal Wounds" (2022). *USF Tampa Graduate Theses and Dissertations*.
<https://digitalcommons.usf.edu/etd/9468>

This Dissertation is brought to you for free and open access by the USF Graduate Theses and Dissertations at Digital Commons @ University of South Florida. It has been accepted for inclusion in USF Tampa Graduate Theses and Dissertations by an authorized administrator of Digital Commons @ University of South Florida. For more information, please contact scholarcommons@usf.edu.

A Protein-Based Therapeutic Combination for the Treatment of Hard-to-Heal Wounds

by

Graham L. Strauss

A dissertation submitted in partial fulfillment
of the requirements for the degree of
Doctor of Philosophy
Department of Medical Engineering
College of Engineering
University of South Florida

Major Professor: Piyush Koria, Ph.D.
Nathan Gallant, Ph.D.
Mark Jaroszeski, Ph.D.
William Lee, Ph.D.
Martin Muschol, Ph.D.

Date of Approval:
June 30, 2022

Keywords: Recombinant Technology, Mesenchymal Stem Cells, Protease Inhibitor, Chronic
Wound, Inverse Phase Transitioning

Copyright © 2022, Graham L. Strauss

Dedication

This work is dedicated to my fiancé, Amanda McCarthy, and my parents, Leonard and Greta Strauss for their unwavering support of my educational and professional pursuits.

Acknowledgments

I would like to extend a sincere thank you to Dr. Piyush Koria and Truman Roland for their support and assistance in my research.

Additionally, I would like to acknowledge the Florida High Tech Corridor Council for their monetary contribution to some of this work.

Table of Contents

List of Tables	iii
List of Figures	iv
Abstract	vii
Chapter 1: The Clinical and Economic Burden of Chronic and Hard-to-Heal Wounds	1
Chapter 2: Fusion Protein Construction and Expression	10
2.1 Materials	10
2.2 The Construction of Recombinant ELP Fusion Proteins	10
2.3 Expression and Purification of ELP Fusion Proteins	13
Chapter 3: Verification of pI-Based Phase Separation for the Purification and Application of ELP Fusion Proteins	15
3.1 Hypothesis Behind the Charge Dependency of ELP Transitioning	16
3.2 Quantifying ELP Fusion Protein Transitioning Utilizing Absorbance Measurements	19
3.3 Dynamic Light Scattering Experiments	20
3.4 Absorbance Results for pI-BPS of ELP Fusion Proteins	20
3.4.1 Sources of Error and Variability	22
3.5 Dynamic Light Scattering Analysis of Particle Size Formation During PI-BPS	25
3.6 Implementation of a Matrix-Tethering ELP Fusion Protein	30
Chapter 4: Dual Inhibitory Activity of PMPD2-L10Flag-APPIP of Elastase and Matrix Metalloproteinase-2	32
4.1 Methods for the Determination of PMPD2-L10Flag-APPIP's NE Inhibitory Activity	32
4.2 Methods for the Determination of PMPD2-L10Flag-APPIP's MMP2 Inhibitory Activity	33
4.3 NE Inhibitory Activity of PMPD2-L10Flag-APPIP	35
4.3.1 NE Inhibitory Activity of PMPD2-L10Flag-APPIP Compared to the Single Fusions	36
4.4 MMP2 Inhibitory Activity of PMPD2-L10Flag-APPIP	39
4.4.1 MMP2 Inhibitory Activity of PMPD2-L10Flag-APPIP Compared to the Single Fusions	41
4.5 Dual and Simultaneous Inhibition of NE and MMP2	44
4.6 Statistics and Sources of Error in the Inhibition Experiments	45

Chapter 5: Mesenchymal Stem Cells and Their Ability to Condition Media Into a Potent Proliferation Inducing Cocktail.	46
5.1 Culturing of Mesenchymal Stem Cells.....	48
5.1.1 Harvesting Um-MSC Conditioned Media	48
5.1.2 Processing the Um-MSC Conditioned Media.....	49
5.1.3 Verification of Um-MSCs.....	49
5.2 Screening Um-MSC Conditioned Media for Inducing Cellular Proliferation.....	53
5.2.1 Proliferation Experiments Utilizing C2C12 Cells in a Serum-Free Environment.....	53
5.2.2 Proliferation Experiments Utilizing C2C12 Cells Treated with MSC-CM and NE	54
5.3 Induction of Proliferation of C2C12 Cells Treated with Um-MSC Conditioned Media With or Without the Presence of Proteases.....	55
5.4 Statistical Analysis for the Proliferation Assays.....	59
Chapter 6: An Essential Combination of Protease Inhibition with the Delivery of a Um- MSC Conditioned Media	60
6.1 The Proteolytic Degradation of Therapeutic Proteins	61
6.1.1 The Protection of rhKGF from the Degradation Caused by NE and MMP2	61
6.2 A Chronic Wound Diabetic Mouse Model	62
6.2.1 A Surgical Wounding Procedure	63
6.2.2 NE Pretreatment for Modeling and Inducing a Chronic Wound Environment.....	63
6.2.3 Treating the Mice Wounds with Fibrin Gels Containing the Dual Protease Inhibitor and Um-MSC Conditioned Media	64
6.2.4 Tissue Collection and Histology	65
6.3 Chronic Wound Mouse Model Results.....	66
6.3.1 An Analysis of Wound Epidermal Thickness and Collagen Composition.....	69
6.3.2 Statistical Analysis of Mouse Model Results	73
Chapter 7: Discussion	74
Chapter 8: Key Developments	77
References.....	78
Appendix A: Abbreviation Key.....	80
Appendix B: Copyright Permissions	81
Appendix C: IACUC Approval	82

List of Tables

Table 1	The amino acid sequences for the construction of the ELP fusion proteins.....	10
Table 2	Complete fusion protein sequences and their isoelectric points for each protein studied using pI-BPS	15
Table 3	Experiment groups of the colorimetric NE inhibition assay and their respective components	33
Table 4	Experiment groups of the colorimetric MMP2 inhibition assay and their respective components	34
Table 5	Treatment groups and controls for the chronic wound mouse model.....	65

List of Figures

Figure 1 Steps of the Wound Healing Processes in an Acute Wound.....	4
Figure 2 Sanger Sequencing Results for PMPD2-L10Flag-APPIP.....	12
Figure 3 Sanger Sequencing Results for L10Flag-PLGF.....	13
Figure 4 ELP-Fusion Protein Transitioning Behavior for A) Unfused ELPs, B) Single ELP Fusions, and C) Dual ELP Fusions.....	18
Figure 5 Transitioning Behavior of Dual ELP Fusions Utilizing pI-Based Phase Transitioning.....	19
Figure 6 A Display of the Degree of Transitioning of L10Flag and PMPD2-L10Flag-APPIP a Neutral pH and at the Protein's Isoelectric Point.....	23
Figure 7 Microscopy Imaging of Transitioned PMPD2-L10Flag-APPIP.....	24
Figure 8 Dynamic Light Scattering Data for L10Flag at a 7.4 pH, from 10°C to 30°C.....	27
Figure 9 Dynamic Light Scattering Data for PMPD2-L10Flag-APPIP at a 7.4 pH, from 10°C to 40°C.....	28
Figure 10 Dynamic Light Scattering Data for PMPD2-L10Flag-APPIP at its pI, 4.1 pH, from 10°C to 40°C.....	29
Figure 11 A Total Protein Stain of Samples of L10Flag-PIGF2 and PMPD2-L10Flag for the Evaluation of Affinity of PIGF2 for Various Matrix Proteins.....	31
Figure 12 A Kinetic Absorbance Analysis for Concentrations of PMPD2-L10Flag-APPIP and its Inhibition of NE in the NE Colorimetric Assay.....	35
Figure 13 A Display of NE Inhibition, in % Inhibition, by the Dual Inhibitor, and the Single Fusions.....	36
Figure 14 A Kinetic Absorbance Analysis for Concentrations of the Single Fusions, A) PMPD2-L10Flag and B) L10Flag-APPIP and Their Inhibition of NE in the NE Colorimetric Assay.....	38

Figure 15	A Kinetic Absorbance Analysis for Concentrations of PMPD2-L10Flag-APPIP and its Inhibition of MMP2 in the MMP2 Colorimetric Assay	40
Figure 16	A Display of MMP2 Inhibition, in % Inhibition, by the Dual Inhibitor, and the Single Fusions	41
Figure 17	A Kinetic Absorbance Analysis for Concentrations of the Single Fusions, A) PMPD2-L10Flag and B) L10Flag-APPIP and Their Inhibition of MMP2 in the MMP2 Colorimetric Assay	43
Figure 18	The Simultaneous Activity of Each Bioactive End of PMPD2-L10Flag-APPIP in a Kinetic Inhibition Assay Containing MMP2 and NE	45
Figure 19	Flow Cytometry Results of Um-MSCs Targeting the Expression of Each Positive Marker for Mesenchymal Stem Cell Determination.....	51
Figure 20	Flow Cytometry Results of Fully Stained Cells Without DAPI to Determine the Degree of Negative Marker Expression	52
Figure 21	The Proliferation of C2C12 Cells Treated with Various Collections of Um-MSCs Conditioned Media.....	57
Figure 22	The Degradation of MSC Conditioned Products by Various Concentrations of NE.....	58
Figure 23	Um-MSCs Conditioned Media in Various Treatment Forms Tested for Inducing Proliferation of C2C12 Cells	59
Figure 24	A Western Blot Analyzing the Protection from Degradation of RhKGF in the Presence of NE and MMP2 Over a 24-Hour Incubation	62
Figure 25	Representative Images of the Mice Wounds from the NE Pretreated Controls Taken at the Experiments End Point.....	67
Figure 26	Representative Images of the Mice Wounds from the Experimental Groups that were NE Pretreated and then Received MSC Conditioned Media Treatments with Continuous NE Treatments	67
Figure 27	Representative Images of the Mice Wounds from the Experimental Groups that were NE Pretreated and then Received MSC Conditioned Media and PMPD2-L10Flag-APP with Continuous NE Treatments	68
Figure 28	Representative Images of Masson's Trichrome Stained Wound Tissue Samples	71

Figure 29 The Average Epidermal Thickness from Tissue Samples Collected from Each Mouse Group Measured in ImageJ and Normalized to the Untreated Control72

Figure 30 Collagen Composition of the Mice Wounds Normalized to the Collagen Composition of the Untreated Control.....73

Abstract

Chronic wounds present many clinical challenges in relation to the successful treatment and closure of the damaged tissue. Most current treatment methods focused on one or two aspects to drive wound closure, while most chronic wounds are multifactorial environments with many of those dependencies relying on the termination of one another to effectively gain tissue construction, closure, and full skin thickness and composition. Natural wound healing processes allude to potential biologics that can impede the chronic breakdown of tissue, while restoring deposition of new tissue, and effectively leading to a healed wound. Proteases secreted by the body's immune system lay waste to even the healthy tissues in wounds, which can be seen in those that turn chronic, as a progressive and persistent break down of tissue, proteins, and cells in the wound site. The disruption of this exacerbated tissue breakdown is both essential to quell the destruction of healthy tissues as well as other proteins such as growth factors that are needed to signal for the development and deposition of new tissue. The latter points to the importance of the balance between tissue break down and deposition, commonly referred to as remodeling, as a focusing point for the healing of chronic wounds. The two generalized secreted molecules that balance tissue breakdown and deposition are proteases and growth factors respectively. However, the efficacy of growth factors that exist in a wound site are highly dependent upon the concentration of secreted proteases. Therefore, in chronic wounds the proteases which are continuously secreted, without intrinsic inhibition, will chew up the growth factors responsible for signaling deposition, which causes tissue destruction to be the overpowering and vicious result. The protein-based combination therapy created here works to rebalance tissue breakdown and

deposition to tend toward minimal deconstruction with overpowering construction. It works by inhibiting proteases, flooding the site with many growth factors, while also sustaining the presence of the treatment over longer periods to avoid site disturbance and leakage of the biologic combination into neighboring tissues. This protein combination is a powder-based freeze dried therapeutic, that can be used in powder form or reconstituted into many mediums and materials for desired application and results. It is a multifunctional treatment, with the main controlling factor for application being wound size as a governing guideline for dosage, as it can be applied in many different forms such as raw powder, liquid, gel, and in materials for an application tailored to the characteristics of the treatment site.

Chapter 1: The Clinical and Economic Burden of

Chronic and Hard-to-Heal Wounds

Wound care and the impact of a growing population presenting delayed wound healing has been an enormous conversation for decades regarding its economic and clinical impacts. Despite widespread concern, it has been observed that the treatment of chronic wounds has not advanced beyond rudimentary techniques to help spike wound closure and minimize the progression of other diseases that accompany wounds, such as infection. Infection remains a heavy collateral burden when treating hard-to-heal wounds (HtHWs). The longer a wound stays open, the greater the opportunity for bacteria to establish around the nutrients of a gaping wound. Once established, infection perpetuates the issue of chronicity through the breakdown of healthy tissue into bacterial nutrients. Both the clinical and economic success of a chronic wound is a time dependent issue, where the time it takes to close a wound determines the primary outcome of how hard to heal the wound may be through the addition of further tissue insult and is directly related to the clinical commitment and economic requirements to utilize therapies long term to eventually obtain wound closure.

Chronic and HtHWs affect a broad range of patient demographics and age groups either affected by associated diseases that lead to HtHWs or due to physical and environmental impacts from lifestyle activities. It is seen that over a decade ago, in 2009, 6.5 million patients in the United States presented chronic wounds, racking up an annual treatment bill of \$25 billion dollars¹. While in 2018, targeting an “at risk” population, an analysis of only Medicare beneficiaries reported 8.2 million patients being treated for wounds with an estimated range of total costs to treat being

roughly \$28 - \$97 billion². With current statistics and economic impacts being a complex analysis, the observational truth that underfunding wound care research and poor regulation in regenerative medicine industries, shed light on the fact that wounds continue to progress in impact, but nothing has been successfully developed and translated to shunt the impact of HtHWs, in a downward projection, on both the patient and the economy. In fact, as recent as 2021, the Department of Defense (DOD) has published white papers regarding combat wounding being the leading cause of death on the battlefield, stating that affordable therapeutics have not yet been made to withstand the hardships of healing a wound in the field³. In further analysis the DOD believe that wound healing has been underfunded, underdiscussed, and products have been inhibited from translation into the market in a timely and cost-effective manner³. The latter places an important aspect of healing hard-to-heal wounds and that is the impact local environmental factors have on wound healing. An expansion of this idea is that even weather-related environmental factors may elevate the risk to develop a HtHW. For example, tropical environments, which can be wet and warm, act as perpetuators of chronic wounds as the climate is more favorable for the spread and establishment of bacteria within a wound. An understanding of who, where, and when in the wound healing phase seems to be the foundational factors of successfully healing a delayed wound. However, the more important factor is quite simply the inner environment of the wound, since human tissues all heal the same way, if wound closure is achieved before time dependent factors like who the patient is and what the environment they live in and how it exacerbates issues in the wound healing process. This understanding is essential when developing wound care products because the process of treating the wound can then be strikingly universal. With the right product, and clinician focus on eliminating the complexities of the problem, can be accomplished by simply focusing on

interrupting the awry system shunting the bodies response to a wound and ultimately moving it toward the remodeling phase.

A chronic wound has been commonly defined as a wound that fails to heal within a three-month period⁴. But, from a physiological perspective, a chronic or HtHW is simply a wound where the healing process halts within a tissue deconstruction phase, while never establishing new healthy tissue and structure⁴⁻⁶. The latter happens well before the 3-month classification making intervention an immediate need rather than a need at the three-month mark. On the surface of the body, a proper wound healing process, from damage to closure, consists of 4 simplified phases. The normal wound healing is shown in Figure 1. Upon tissue trauma the first phase of healing is hemostasis and blood clot formation followed by inflammation and tissue breakdown queued by stimulated and migrated immune cells in the wound site. Once the damaged tissue is degraded the wound quickly enters the third phase where cellular migration and proliferation of healthy tissue occur. The fourth and last phase of a healthy wound healing cycle consists of tissue remodeling where the wound is closed, and tissue architecture is completely restored. HtHWs remain in the step where tissue breakdown and tissue clearance, seen by the governing immune system, as most important. This is due to the overabundance of proteases secreted by local cells, essentially causing a vicious cycle where tissue deconstruction overpowers tissue reconstruction leading to a festering open wound.

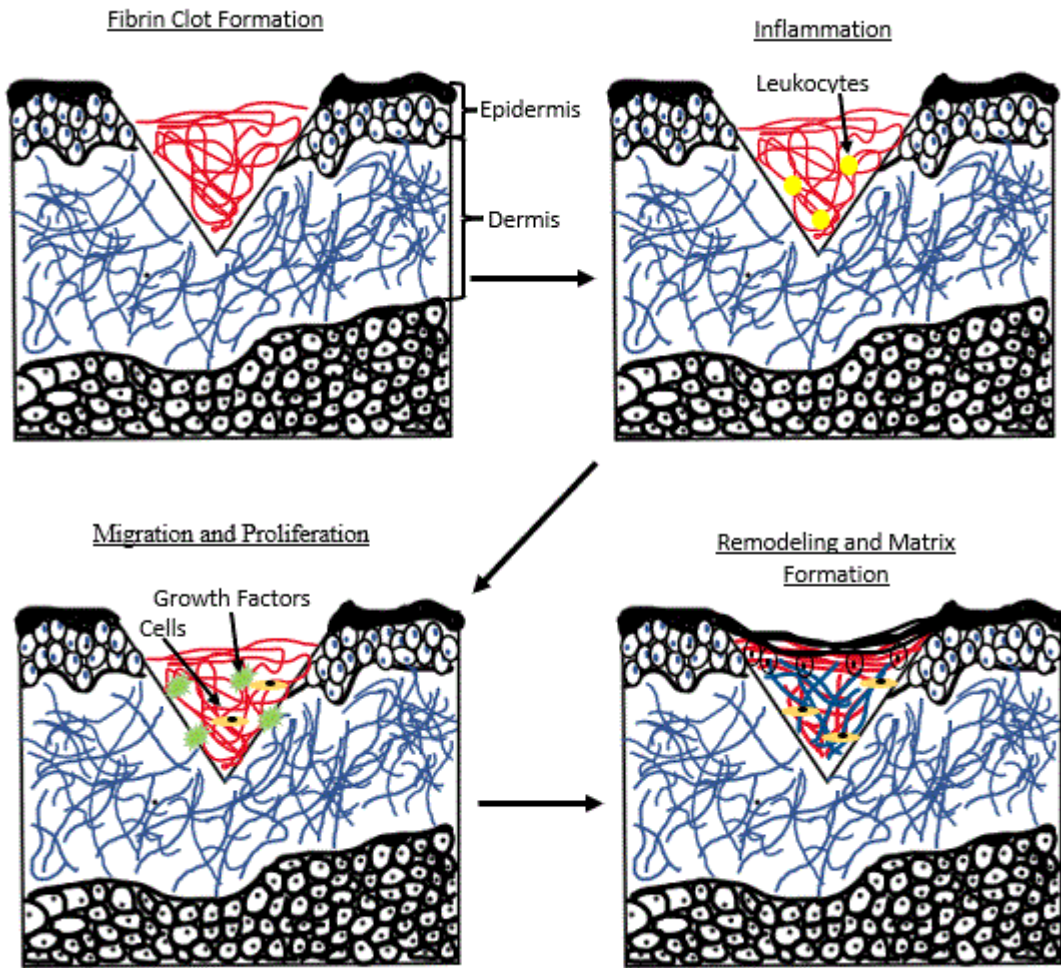


Figure 1. Steps of the Wound Healing Processes in an Acute Wound

Current treatments for delayed wounds have been around for decades and remain basic. Treating a persistent wound normally takes the initial form of a clinician’s understanding of why a patient presents a chronic wound^{7, 8}. This is a systemic evaluation of overall health, pinpointing connected diseases like diabetes and heart disease, where the symptomatic characteristics of these diseases are linked to why a wound may not be healing. Additionally, immunological disorders, or a body’s self-infliction of damage, can hurl the normal wound healing process into a cycle where tissue is constantly broken up in the wound site, while never establishing the steps necessary for

tissue reconstruction⁹. The very nature of a systemic outlook on a HtHW can be overwhelming for clinicians and though a systemic disease may be the forefront contributor to the formation of a wound with delayed healing, it must never be treated as the main cause. It may be completely necessary to manage systemic diseases that support HtHW formation, or impede closure, but a chronic wound may never heal just by a clinician's focus on diminishing a contributing disease but rather keeping a costly wound open while doing so. The root cause is simply a local imbalance, in the wound site, causing tissue breakdown to supersede tissue reconstruction^{6, 7, 10-13}. The focus for healing HtHWs should be placed on restoring this imbalance and closing the wound fast to minimize widespread burden on the patient and the economy. Then managing systemic problems become important as they may contribute to a healed wound's relapse back to chronicity.

Traditional treatment methods still hold their place as valuable procedures and therapies to aid in wound closure. Debridement, which is a removal of dead tissues from a wound is a necessary step, not for the immediate healing of the wound, but rather for optimal delivery of effective therapeutics. The treatment of chronic or HtHWs may, by necessity, include antibiotics to rid the wound site of bacterial infection. But again, this is a secondary method of therapy where the primary focus, restoring balance in tissue breakdown and tissue construction, will close a wound fast and further prevent time for secondary contributors to delayed wound healing. The body's immune system and cellular response are responsible for the breakdown of damaged tissue through the secretion of proteinases that target the tissue's structural components and delay healing¹². This is a complex process that involves different cell types and their associated protease secretions, but it is well known what secretions are responsible for the breakdown of different tissue types like neutrophil elastase (NE) and matrix metalloproteinase-2 (MMP2)^{7, 14, 15}. An added aspect of tissue degradation in chronic and HtHWs is an established bacterial infection leading to

further proteolytic degradation^{10, 12, 16}. Bacteria secrete their own metalloproteinases to aid in a competitive establishment and acquire the nutrients necessary to expand and take over a wound site^{5, 7}. However, this displays commonality across two different contributing factors to HtHWs. That is in one case it is our body oversecreting tissue degrading enzymes, and in the case of bacteria they also secrete tissue degrading proteases to survive, grow, and compete. The latter draws importance to the fact that it does not matter what the case is, the result is tissue breakdown. Inhibiting tissue breakdown is absolutely key in pursuing closure of a delayed wound and can be done easily by targeting secreted proteases that are commonly found at high levels in chronic wounds. Tissue construction is heavily reliant on the secretion of protein growth factors which contain an important role in cell migration, proliferation, and cellular matrix secretion¹⁷. However, the same proteases that break down wounded tissue, also wreak havoc on any proteins present in the site¹⁸, which includes the very important growth factors needed to remodel. The prior will keep the wound halted in a deconstruction phase. Without the necessary growth factors present, cellular migration and proliferation will happen on a very low level if not at all. The proteases present in chronic wounds destroy healthy tissue and viable signaling proteins, ultimately halting the normal wound healing process in a vicious loop that only focuses on deconstructing the wound site.

The problem described here can be answered with the replacement of biological switches that aid in progressing the wound further in the healing cycle. This can be done utilizing protein-based protease inhibitors^{12, 13, 18}. Once protease inhibition is established, the risk of proteolytic degradation of tissue and useful growth factors is minimized, then the HtHW can move forward into the remodeling phase, where signaling for migration and proliferation can occur minimizing destruction of the signaling molecules. Here, protease inhibitors are the “off-switch” to the vicious cycle of tissue degradation in a in a wound with delayed healing, while the “on-switch” is the

addition of growth factors and cytokines that can aid in remodeling. However, it is critical that both “switches” exist together as they are mutually beneficial to progressing the wound toward closure. The protease inhibitors protect the tissue and additionally the growth factors, since the phase of wound healing cannot move forward without proper signaling from the growth factors. Once both effects are established, together, the HtHW will progress towards closure.

A wound healing strategy to target hard-to-heal wounds was formulated to interrupt this system of balance of tissue destruction and deposition, while keeping in mind the economic impacts and inherent burdens the current treatment of chronic and HtHWs incur. A protein-based therapeutic was designed as a three-component system that includes a multifunctional protease inhibitor, a conditioned media for inducing cellular proliferation, and an additional extracellular matrix binding protein to target and extend delivery of the protease inhibitors around essential tissue structures that are susceptible to proteolytic degradation. While keeping in mind factors related storage and ease of use of a product, it was created to be a freeze-dried, powder-based product, with an extended shelf-life, and ease of application of a powdered product that for example is less affected by factors such as gravity on a flowing liquid. Additionally, the three-component system is made and processed in a way where there exist only 3 components to synthesize and then mix. Each of the three components inherently include multiple functions. Therefore, instead of making a three-component system with three functionalities, this is a three-component system with many more than three functionalities without adding additional systems or steps to acquire them. In other words, this product can be made with 3 bioreactors and then

mixed, rather than 10+ bioreactors to gain each functionality through inherently separate systems, which drives down cost and time to produce.

Through clinical evidence the proteases to be targeted by the 1 component, multifunctional inhibitor were human neutrophil elastase (HNE) and matrix metalloproteinase-2 (MMP2)^{11, 12, 14, 18, 19}. The utilization of an elastin-like peptide (ELP) core centered between two corresponding protease inhibitors, PMP-D2 and APP-IP, respectively, is essential to create an easily editable and expandable platform, which can be synthesized and purified rapidly while maintaining unique bioactivities of each region. The ELP serves multiple functions, the two most important being self-assembly for purification via inverse phase transition (ITC) and application, while an additional important function of the ELP is to serve as a molecular spacer between unique biologically active regions that must contain availability and spatial requirements for proteases to bind, and for the inhibitors to act specifically and simultaneously on target proteases. However, ELP fusion proteins created in this manner are incredibly hard to purify, if not impossible to purify any considerable amount of peptide due to repulsive forces of similarly charged bioactive ends. Therefore, a process established by the authors has been applied and denoted as pI-Based Phase Separation (pI-BPS), which utilizes pH changes to neutralize repelling charges that make self-assembly and therefore purification impossible at a neutral pH. This challenge and solution give way to another potential loss of functionality at the level of therapeutic application. ELP fusions have traditionally been utilized to create a sustained release of the therapeutic, since they will assemble and aggregate at body temperature²⁰. However, if a constructed protein cannot be purified effectively at a neutral pH utilizing ITC, then it most definitely won't self-assemble in the application site due to these charge hinderances, if not transitioned at a pH close to the protein's pI. Given this new problem and the pursuit to create a product that can be site specific and minimize treatment repetitions, an

additional ELP fusion protein was created to aid in the sustained release and low diffusivity of the product.

A hybrid tethering protein was constructed and added to the dry wound healing product to act as a molecular tether that spans from the inhibitors' ELP regions to binding regions on extracellular matrix (ECM) proteins. Consisting of a placental growth factor (PIGF-2), known for affinity to ECM proteins²¹, and a free ELP end, the binding protein can act as a tether with the protease inhibitor fusion proteins, when the dual protease inhibitor cannot effectively self-assemble. This acts as a fail-safe for maintaining protease inhibitor in the wound bed, and around the ECM that is drastically affected by high concentrations of proteolytic enzymes, thus maintaining the components that are already present, and healthy, while cellular migration and proliferation is elevated by the protein cocktail.

Furthermore, a proliferation inducing component, possibly containing a soup of well-known wound healing peptides and proteins²² secreted by umbilical cord derived mesenchymal stem cells ultimately exists as a blend of freeze-dried peptides that can be applied to a wound to spike proliferation and remodeling. Utilizing synthesis and processing protocols established by the author, allows for the production of a highly potent and consistent mesenchymal stem cell conditioned media. Challenges with culturing mesenchymal stem cells for this purpose include slow doubling rates, low-passage senescence, and variability in resulting conditioned medias. However, through established screening methods for proliferation induction, a culturing process was established, and useful biproducts of UM-MSCs can be used to effectively to cause proliferation and aid in the closure of a wound if protected from the powerful effects of proteases.

Chapter 2: Fusion Protein Construction and Expression

2.1 Materials

Plasmids containing the genes for L10-Flag, PMP-D2, APP-IP, and PIGF2 were obtained from GenScript[®], optimized for corresponding cutting sites for the restriction enzymes PflMI and BglI to exclude cuts within the genes of interest, and includes a gene for resistance to carbenicillin for effective colony isolation. Restriction enzymes (PflMI & BglI) and ligase for the recombinant process were obtained by New England Biolabs[®] Inc. Table 1 displays the amino acid sequences for the correlated genes of interest ordered in pUC57 or pUC19.

Table 1. The amino acid sequences for the construction of the ELP fusion proteins

L10-Flag	((VPGVG)2(VPGLG)(VPGVG)2)10
PMP-D2	EEKCTPGQVKQQDCNTCTCTPTGVWGCTLMGCQPA
APP-IP	ISYGNDALMP
PIGF2	RRPKGRGKRRREKQRPTDCHL

2.2 The Construction of Recombinant ELP Fusion Proteins

The ELP fusion proteins used in this therapeutic mixture were constructed using cloning and recombinant technology in microorganisms. Described by the author prior¹³, pUC57 and pUC19 plasmids containing PMP-D2, APP-IP and L10-Flag were cloned in Top10 and purified to a desirable working concentration for recombinant processes. The plasmid containing L10-Flag was linearized using the restriction enzyme, PflMI. PMP-D2's nucleic acid sequence was cut out

of the pUC57 plasmid utilizing both restriction enzymes, PflMI and BglI, and purified to obtain a PMP-D2 fragment. The PMP-D2 fragment and the linearized pUC19 L10-Flag plasmid were then spliced together utilizing recursive directional ligation to obtain the circular plasmid, PMPD2-L10Flag pUC19. After cloning an isolated bacterial colony containing the new plasmid, PMPD2-L10Flag pUC19, the nucleic acid sequence for PMPD2-L10Flag was fragmented out of the pUC19 plasmid. APP-IP in a pUC57 plasmid was linearized and a recursive directional ligation was performed to yield PMPD2-L10Flag-APP-IP in a pUC57 plasmid. The gene of interest was then double cut using PflMI and BglI, then spliced into a linearized pET25b plasmid for expression in BLR(DE3) e coli.

The nucleic acid sequence for L10Flag-PIGF2 was made similarly to that of the inhibitor. It was designed so that the ELP region is free for tethering to other proteins. A pUC57 plasmid containing the gene encoding for the PIGF2 protein was linearized. Simultaneously, L10-Flag was fragmented out of a pUC19 plasmid. A recursive directional ligation was performed between L10-Flag fragment and the linearized PIGF2 pUC57. The resulting circular pUC57 plasmid contained the gene encoding for L10Flag-PIGF2. L10Flag-PIGF2 nucleic acid sequence was fragmented from the pUC57 plasmid, ligated into a circular pET25b plasmid, and transformed into BLR(DE3) e coli.

All constructed ELP fusion proteins are verified via Sanger Sequencing. The results of Sanger Sequencing for PMPD2-L10Flag-APP-IP and L10Flag-PIGF2 are seen in Figure 2 & 3.

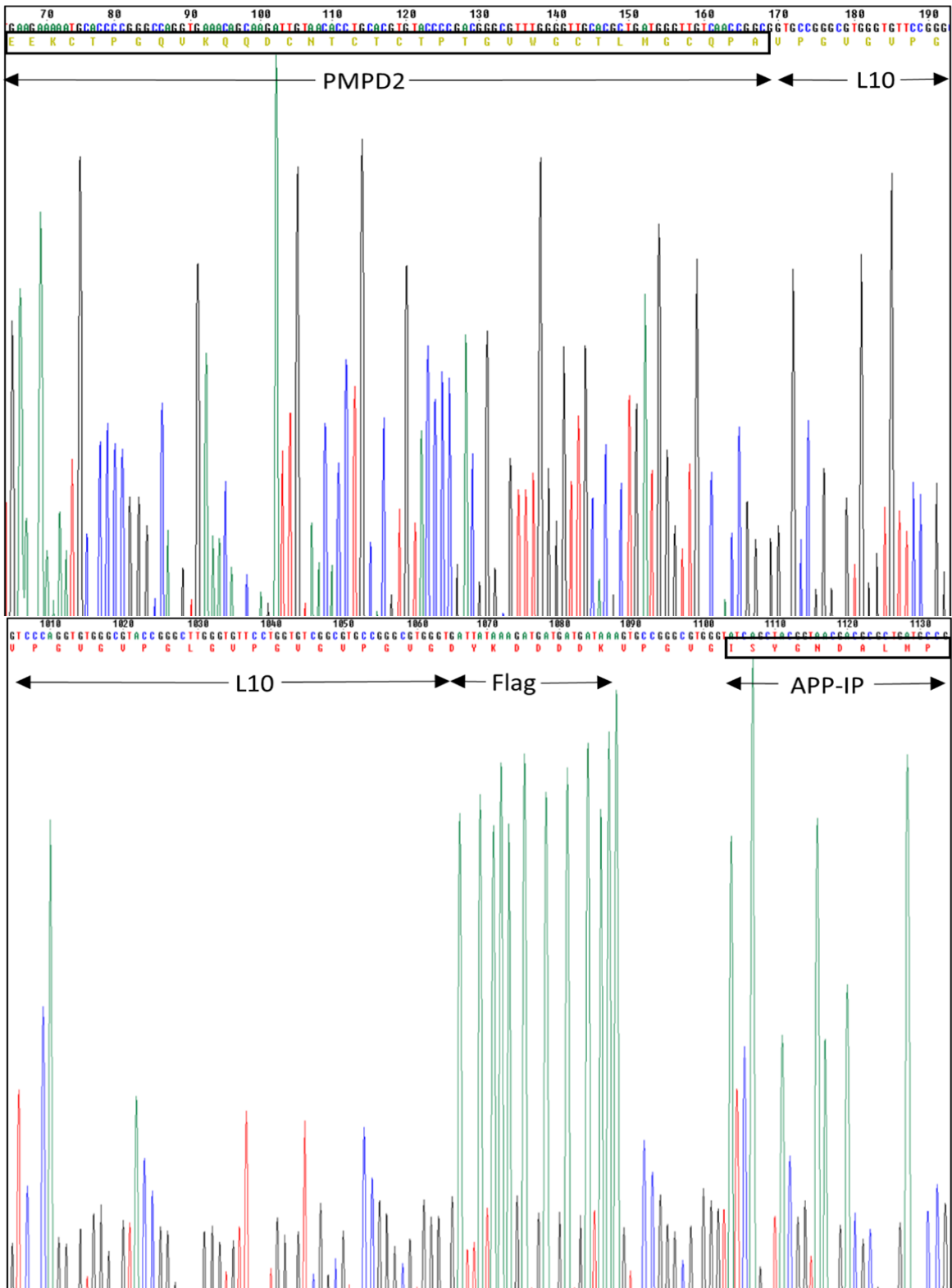


Figure 2. Sanger Sequencing Results for PMPD2-L10Flag-APP-IP. PMPD2 Fused to the N-Terminus of L10Flag. And APP-IP Fused to the C-Terminus of L10Flag

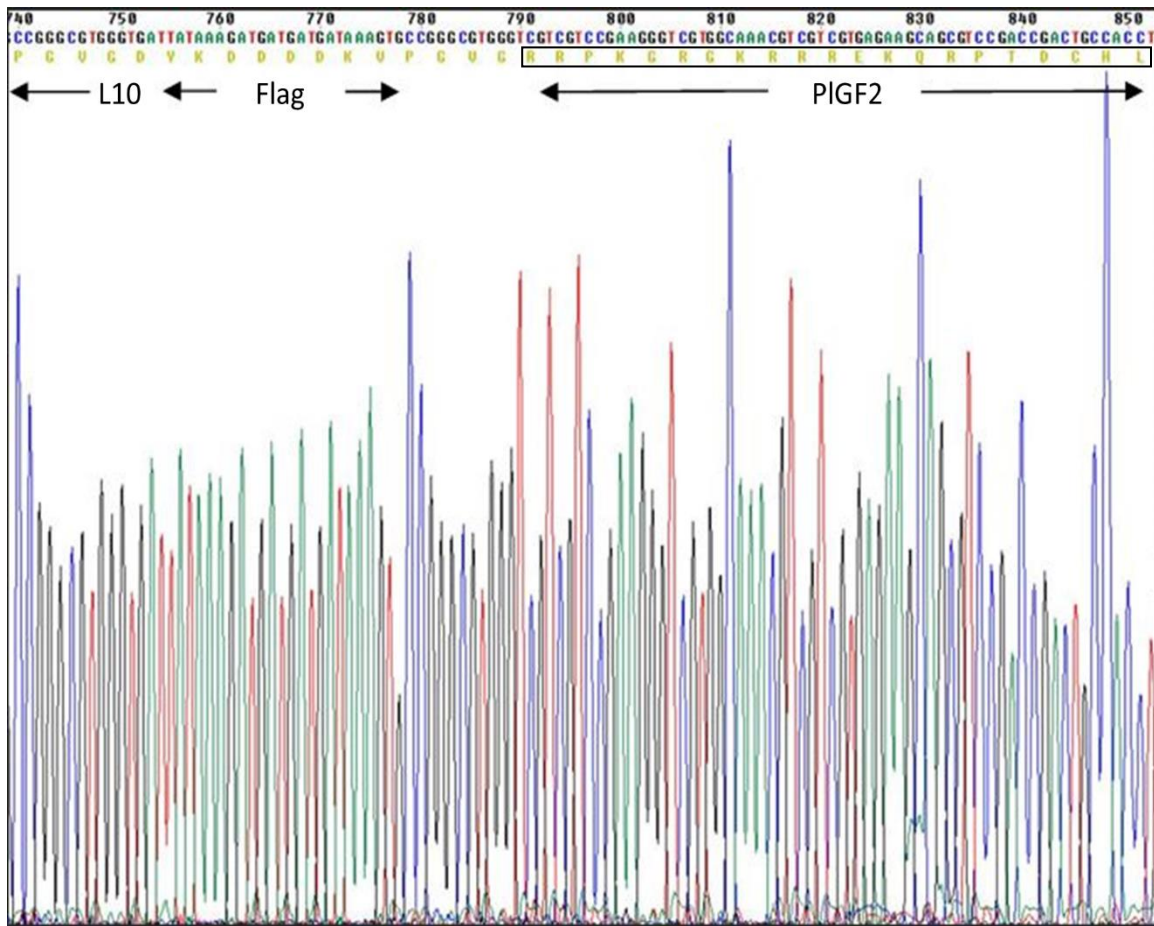


Figure 3. Sanger Sequencing Results for L10Flag-PLGF. PLGF Fused to the N-terminus of L10Flag.

2.3 Expression and Purification of ELP Fusion Proteins

After transformation into BLR(DE3) e coli, a single colony for each desired fusion protein was used to inoculate a separate 75 mL of terrific broth (TB) supplemented with carbenicillin. After 12 hours incubating at 37°C with agitation, the 75 mL for each protein to be expressed and purified was transferred into a liter of TB supplemented with carbenicillin. A 24-hour incubation at 37°C with agitation was performed on each culture. After a 24-hour incubation, the cultures were centrifuged to separate the bacteria containing the expressed proteins from the TB. The

bacterial pellets were each resuspended in 160 mL of cold 1xPBS and lysed utilizing three sonication and mixing steps. Once lysing is complete the protein and bacterial lysate samples were centrifuged at 4°C, twice, to separate the bacterial debris from the solubilized fusion proteins in the supernatants. Inverse Transition Cycling (ITC) is utilized to separate the ELP fusion proteins from debris. ITC begins by the addition of NaCl to each sample to a final 4 molar concentration. It is important to note, a new procedure was implemented into a standard ITC protocol where before a hot centrifugation, the pH of each sample is adjusted to match the pI of each protein, while before a cold spin the pH is adjusted back to a neutral pH or to a pH extreme depending on protein net protein charge. This process is coined pI-Based Phase Separation (pI-BPS), and necessary to obtain useable protein yields when purifying dual fusions, like PMPD2-L10Flag-APPIP. Each sample was placed in a 45°C hot bath for 15 to 30 minutes (depending on how quickly each sample transitions). After hot centrifugation, the transitioned protein pellets were separated from the supernatants, and resuspended in 100 mL of cold 1xPBS. Once evenly resuspended and the pH adjustment is made, the samples undergo a cold centrifugation at 4°C. After the cold centrifugation, the supernatants containing the proteins are collected and separated from the pellets containing debris. The hot centrifugation and cold centrifugation alternation and collection with the appropriate pH adjustments are performed repeatedly until the final protein product is cleared of debris. Once resolved, the final protein pellets are resuspended in 50 mL of deionized H₂O and dialysis is performed for 24 hours. Once dialysis is complete, the protein solutions were then frozen at -80°C and then lyophilized until freeze dried completely.

Chapter 3: Verification of pI-Based Phase Separation for the Purification and Application of ELP Fusion Proteins

Protein charge is based on the charge of each residue that comprises the overall amino acid sequence for a particular protein. Isoelectric point (pI) is a solution pH where a protein exhibits a net zero charge. PI-BPS was verified useful through experimental observation of protein yields resulting from inverse transition cycling, quantification of transitioning at a neutral pH and at a protein's pI evaluated by absorbance over temperature changes, and dynamic light scattering. Table 2 displays ELP fusion proteins, their sequences, and isoelectric point tested in the absorbance-based transitioning experiments, while not all were evaluated by dynamic light scattering.

Table 2. Complete fusion protein sequences and their isoelectric points for each protein studied using pI-BPS

Protein	Sequence	Isoelectric Point (pI)
L10Flag	((VPGVG) ₂ (VPGLG)(VPGVG) ₂) ₁₀ -DYKDDDDK	3.74
PMPD2-L10Flag-APPIP	EEKCTPGQVKQQDCNTCTCTPTGVWGCTLMGCQPA -((VPGVG) ₂ (VPGLG)(VPGVG) ₂) ₁₀ -DYKDDDDK- ISYGN DALMP	4.10
L10Flag-PIGF2	((VPGVG) ₂ (VPGLG)(VPGVG) ₂) ₁₀ -DYKDDDDK- RRPKGRGKRRREKQRPTDCHL	9.35

3.1 Hypothesis Behind the Charge Dependency of ELP Transitioning

Unsuccessful purification of ELP-fusion proteins such as, PMPD2-L10Flag-APPIP, lead to a hypothesis that ELPs centered between two bioactive regions with similar charge polarities are hindered during temperature dependent aggregation and will not self-assemble to a degree necessary for bulk phase separation. Figure 4 displays the ELP self-assembling behavior at a neutral pH, for three different cases of fusions. Figure 4A displays the case where there is a unfused ELP. An ELP without fusions is completely unhindered by charges because the ELP sequence is largely non-polar allowing for easy phase separation at a neutral pH. This can be seen in Figure 4A where the ELPs readily aggregate at a temperature (T) above that of the ELPs' transitioning temperature (T_t). Figure 4B presents a case of ELP fusion that contributes hinderance to the overall behavior of aggregation. This case is a single charged fusion at one end of the ELP. Though ELP transitioning can still occur, the degree of transitioning is controlled by the charge density of the fused domain on the end of the ELP. In Figure 4B the aggregate formed is highly dependent on how close two identically charged ends, from two individual molecules, can get before repulsive charges limit ELP interactions at the core of the aggregate. Additionally, Figure 4C shows another case where there is a charged domain fused to each end of the ELP creating a molecule with a non-polar ELP core and two ends of the molecule containing similar repulsive charges. In this case, at a neutral pH, little to no aggregation will be accomplished when solution $T \geq T_t$ because individual molecules and their ELPs will never get close enough to interact and self-assemble due to the repulsive forces between the ends of each bioactive domain during intermolecular interaction.

The reversable elimination of charges on the ends of ELP-fusion proteins allow for the self-assembly and phase transition necessary to utilize ELPs and their transitioning capabilities for purification and application. PH variations of a protein solution to the protein's isoelectric point

can reversibly neutralize charges to allow for aggregation when deemed useful. For example, for protein purification, inverse transition cycling of ELP-fusion proteins can be utilized when highly charged bioactive ends exist through the employment of pH adjustments before hot centrifugations by adjusting the solution pH to the protein's isoelectric point (pI). This eliminates charges for as long as the pH is at the proteins pI. In Figure 5, this hypothesis is observed, and suggests when a protein solution pH is adjusted to that of the protein's pI, ELP interactions are therefore enabled (when $T \geq T_t$) through the elimination of repulsive charges that exist during an intermolecular interaction at a neutral pH in Figure 4C.

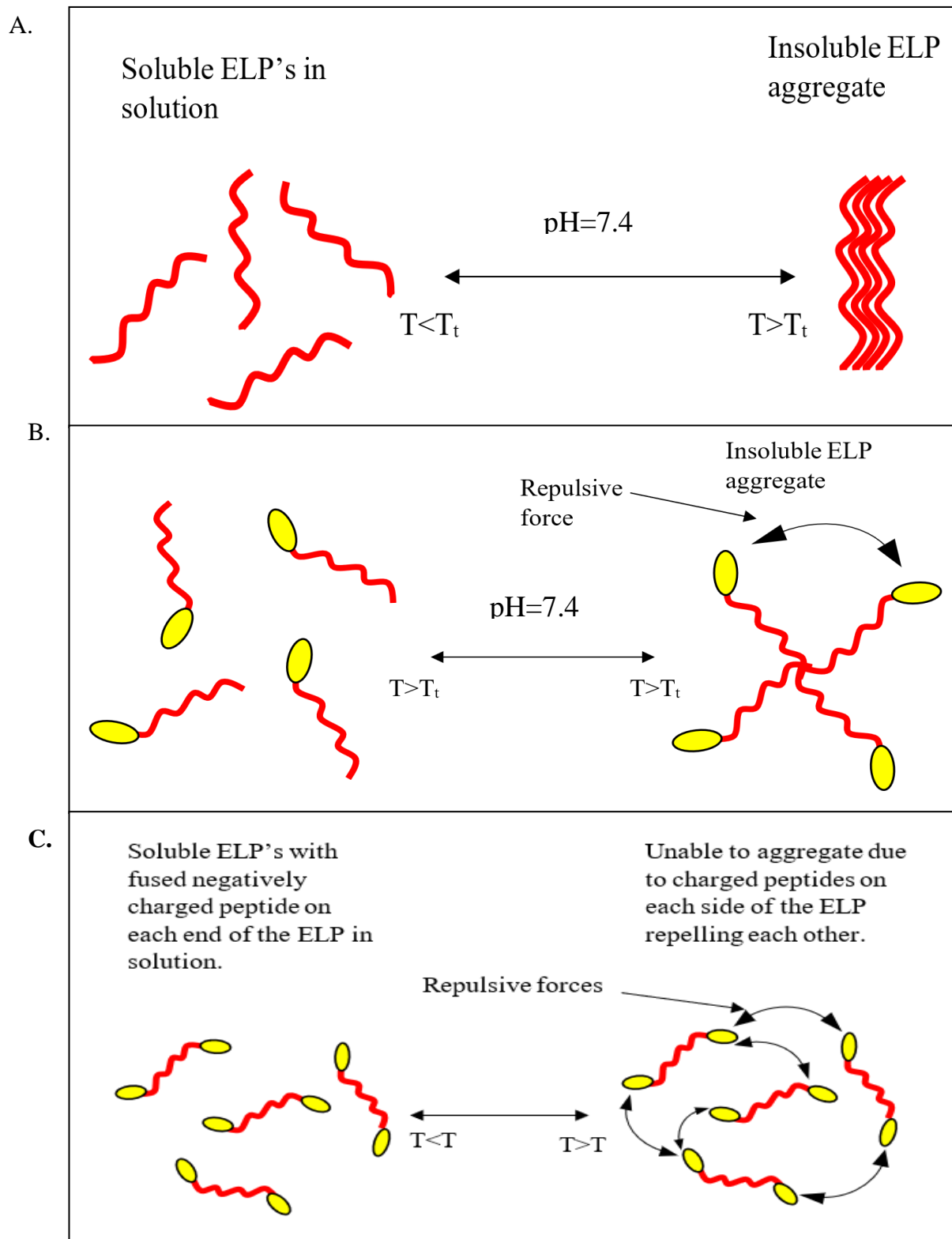


Figure 4. ELP-Fusion Protein Transitioning Behavior for A) Unfused ELPs, B) Single ELP Fusions, and C) Dual ELP Fusions.

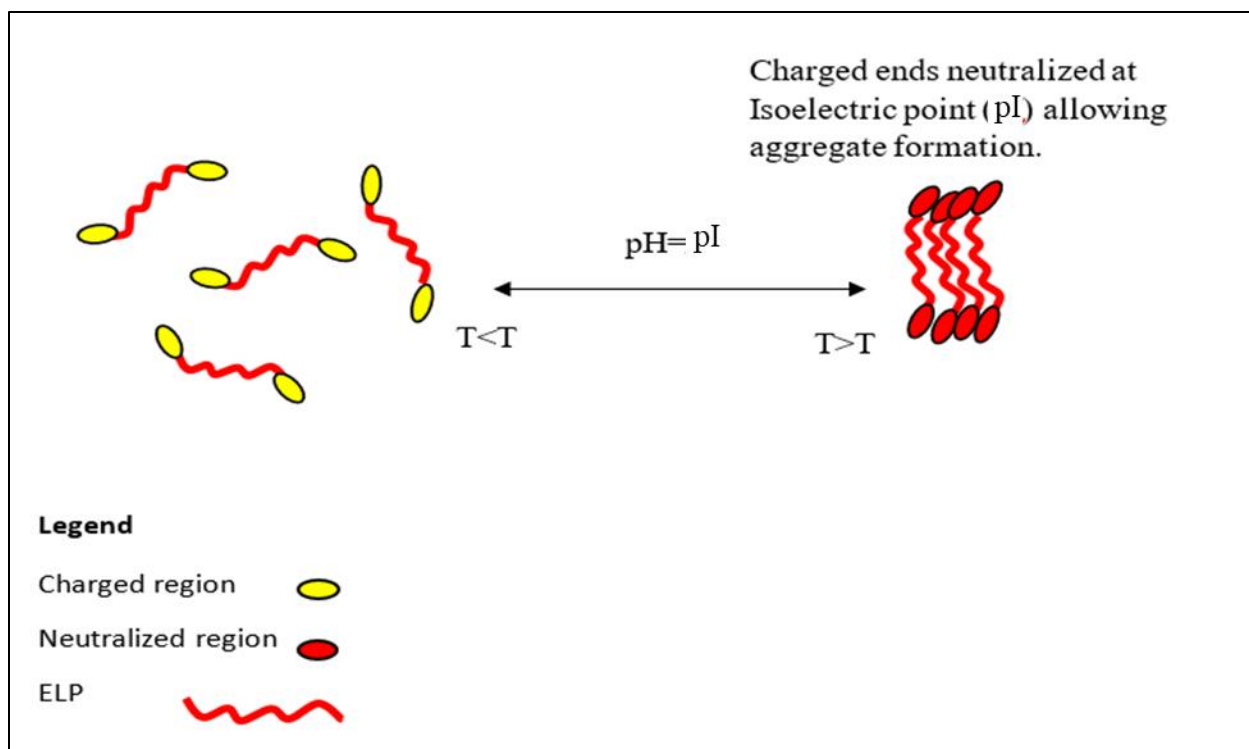


Figure 5. Transitioning Behavior of Dual ELP Fusions Utilizing pI-Based Phase Transitioning.

3.2 Quantifying ELP Fusion Protein Transitioning Utilizing Absorbance Measurements

Various ELP fusion proteins were reconstituted at a neutral pH and at a specific protein's isoelectric point, where the net charge of the entire protein molecule is zero. Utilizing the known amino acid sequences for each ELP fusion protein and an online (isoelectric.org) isoelectric point calculator to calculate the pH where each protein of interest has a zero net charge. The isoelectric point calculator is based upon the use of Henderson-Hasselbach equation, and dissociation constants of positive and negative residues to approximate a protein's charge at a given pH. PMPD2-L10Flag-APPIP and other various proteins were solubilized at its calculated pI and at 7.4 pH. Then in a 96-well plate, the samples were arranged in triplicate. Due to the experimental design and nature of transitioning experiments, correlated blanks of each buffer pH were included. The plate with samples were placed in a BioTek Synergy HT microplate reader, utilizing the software,

Gen5, for a kinetic assay, varying temperature overtime while recording OD₃₆₀. The temperature start point was 30°C and the 96-well plate was preheated to the start temperature before the first reading. The following temperature and read points were at 35, 40, and 45°C. Before each read, there was a delay to account for machine warm up and time for sample transitioning at a particular temperature. Table 2 displays each ELP fusion protein, and their approximate pI used in the purification of these proteins, and in the described experiments.

3.3 Dynamic Light Scattering Experiments

Dynamic Light Scattering (DLS) was performed on samples of both L10Flag and PMPD2-L10Flag-APPIP to better understand the phase separation behavior of these ELP fusion proteins at the protein's isoelectric points and in a neutral pH. A Malvern Zetasizer ZEN 1600, by Malvern Panalytical Ltd., was used to perform all DLS experiments. The DLS protocol was designed to measure size distribution of assembling ELP fusion proteins over a series of temperatures. The protocol begins with a temperature set point of 10°C, then increasing the temperature in 5°C increments with the last DLS measurement at 45°C. After the sample reaches each temperature set point, size distribution and correlogram data was measured and recorded. This experiment is performed on both L10Flag at a neutral pH and PMPD2-L10Flag-APPIP at a neutral pH and at its pI. The resulting DLS data is analyzed in Excel to plot size distribution and associated correlogram data.

3.4 Absorbance Results for pI-BPS of ELP Fusion Proteins

Absorbance measurements of transitioning for ELP fusion proteins confirmed the importance of pI-BPS for the purification and application of these fusion proteins. L10-Flag is the most basic ELP fusion protein that we work with and contains little hinderance to transition since any charge on this protein is from the fusion of a Flag-tag end. Figure 6A represents a graph of

L10 Flag and the degree of transitioning over a range of temperatures at 7.4 and 3.8 pH. Here, it is seen that L10Flag transitions to nearly the same degree at its pI and above its T_t the sample transitions like at a neutral pH. However, at or near L10Flag's transition temperature it is clear that the sample at its pI transitions nearly 5-fold better than at a neutral pH. Figure 6B displays transitioning results of the dual protease inhibitor, PMPD2-L10Flag-APPIP. It is clear that pI-BPS is needed for the ITC purification of this protein. Over the range of tested temperatures, the protein sample at a neutral pH, did not have an elevated increase in absorbance due to transitioning. In fact, the level of transitioning stayed very similar over the tested temperature ranges. At PMPD2-L10Flag-APPIP's pI, 4.1 pH, the transition steadily increased over the range of temperatures reaching a 6-fold increase in absorbance than that of the sample in a neutral buffer.

Through a ITC purification process of PMPD2-L10Flag-APPIP, it was clear that pI-BPS implemented in the ITC protocol was absolutely necessary to maximize protein yield just by observation of end result. Purifying two batches of PMPD2-L10Flag-APPIP alongside one another, with one batch kept at a neutral pH throughout, and the other following pH adjustments for hot centrifugation spins at the proteins PI, further proved the necessity of pI-BPS. The yield in protein for the PMPD2-L10Flag-APPIP, at its pI, was a 22.5-fold increase over the protein yield of the sample that remained at a neutral pH throughout.

Samples of PMPD2-L10Flag-APPIP were further analyzed at the proteins pI and at 7.4 pH. Samples were transitioned and viewed under a microscope to observe size differences in self-assembled particles. Figure 7 A and B show qualitatively the very large difference in particle size when each solution is heated. This observational result further shows the effect of pI-BPS on ELP-based fusion proteins and their transition dependency on solution pH (or protein charge).

3.4.1 Sources of Error and Variability

Standard deviation was calculated for the absorbance experiments and applied to each respective bar of the graphs of absorbance over a range of temperatures. Here in this experiment the propagation of error is likely due to aspects related to temperature range in the microplate reader as temperature is varied. Since the microplate reader heats up from the sides, the center of the plate may be cooler than the edges. To overcome this source of variance the experiment was run utilizing the center of the 96-well plate, while excluding the wells at the edge of the plate. Also, a wait period was utilized to ensure that the entire plate was evenly warmed to the set temperature before a reading was taken.

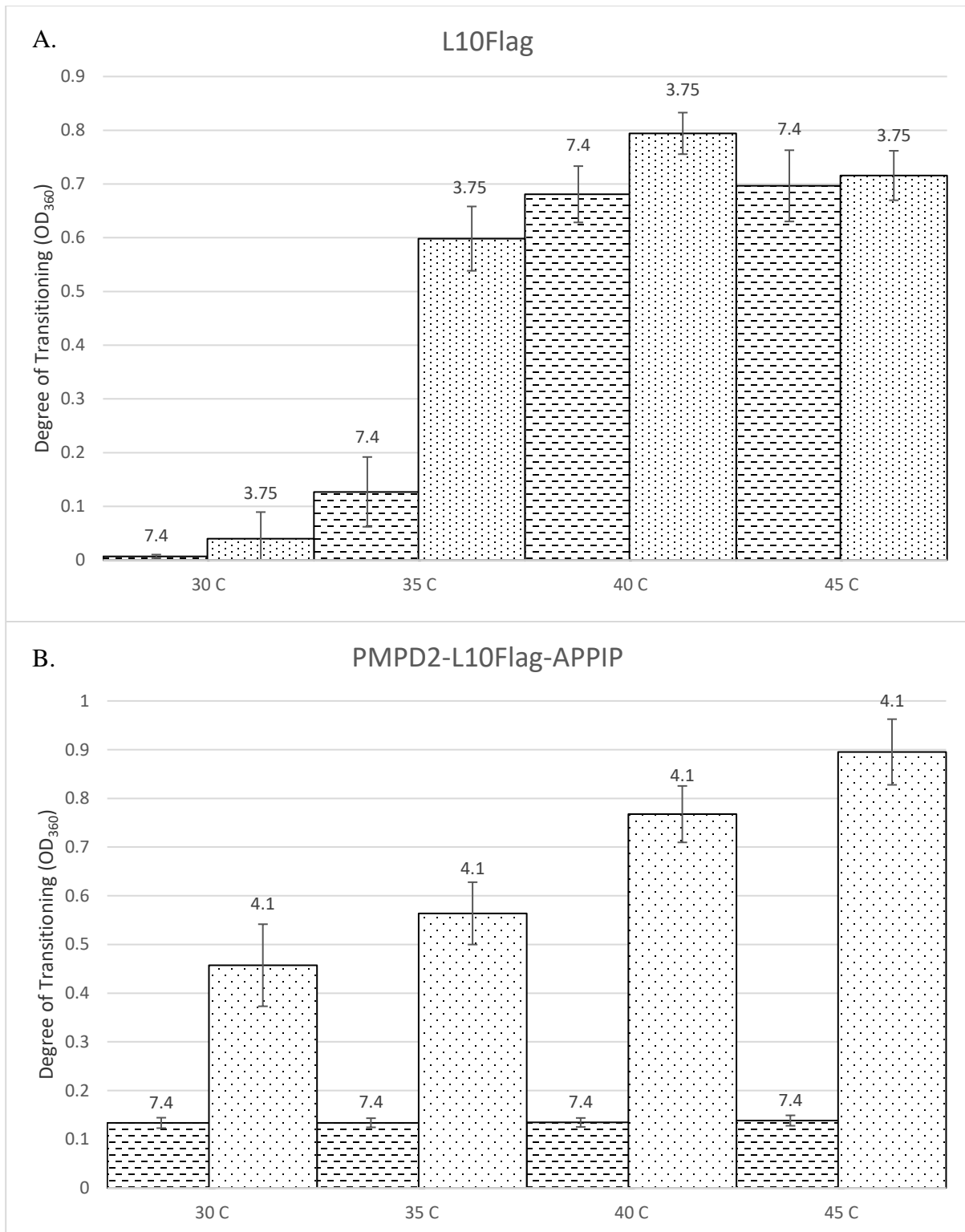


Figure 6. A Display of the Degree of Transitioning of L10Flag and PMPD2-L10Flag-APPIP at a Neutral pH and at the Protein's Isoelectric Point. A) L10Flag at a neutral pH and its pI. B) PMPD2-L10Flag-APPIP at a neutral pH and its pI

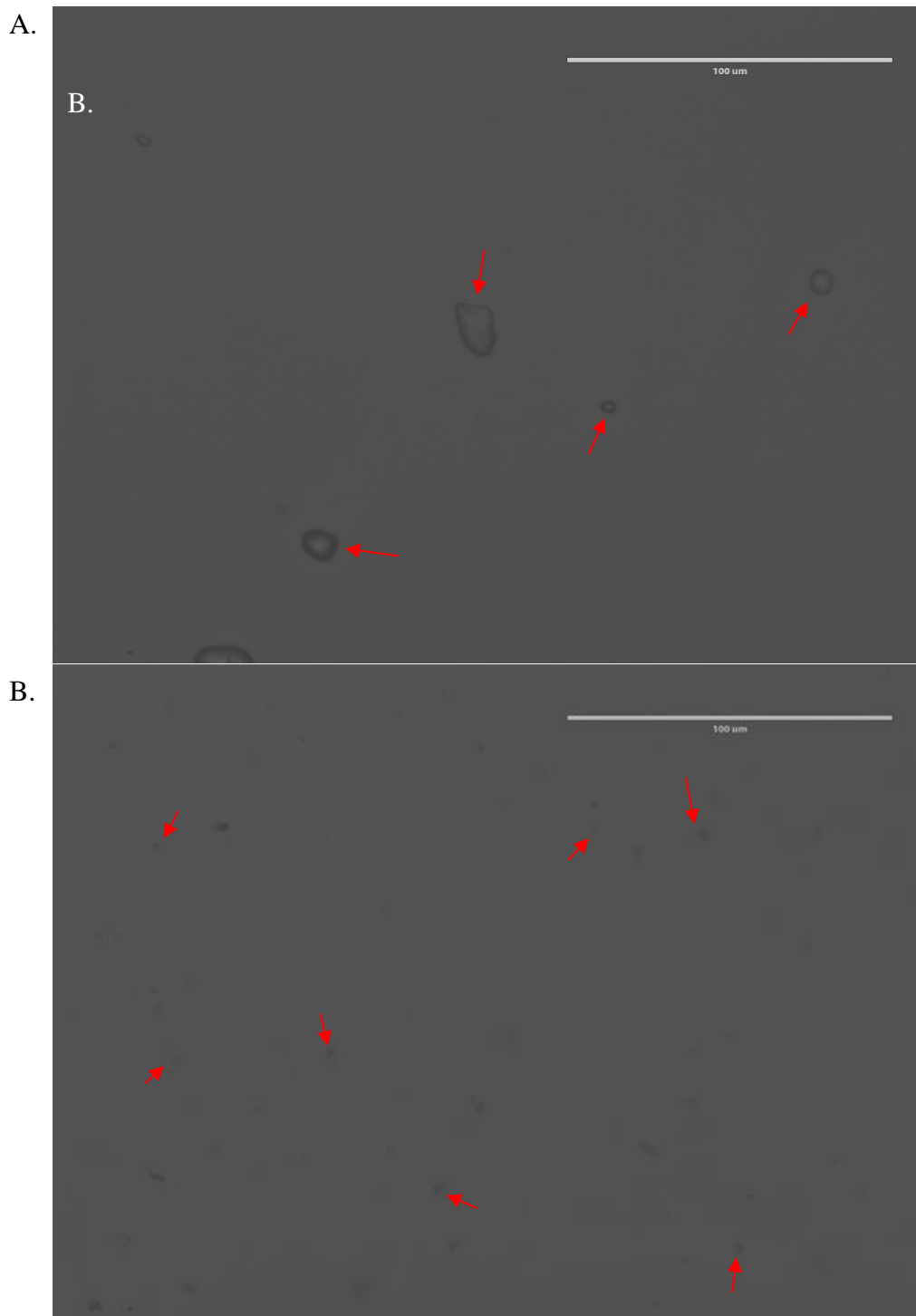


Figure 7. Microscopy Imaging of Transitioned PMPD2-L10Flag-APPiP. A) At PMPD2-L10Flag-APPiP's pI B) PMPD2-L10Flag-APPiP at a neutral pH

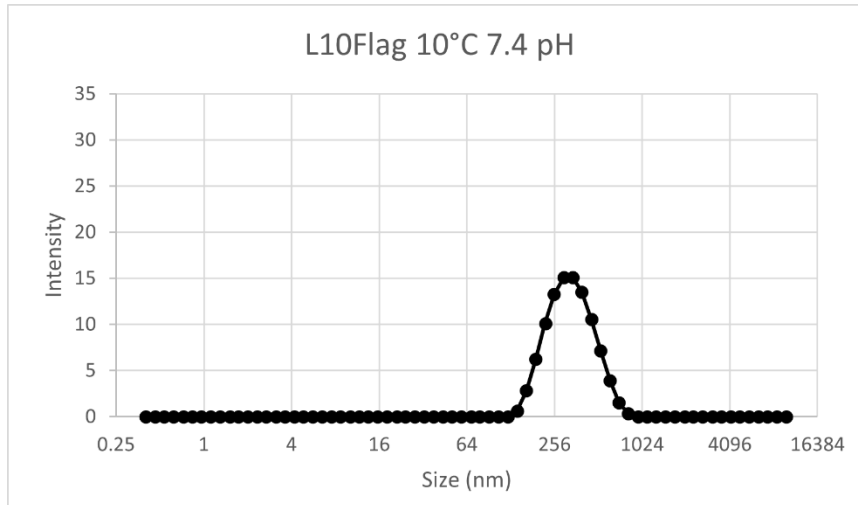
3.5 Dynamic Light Scattering Analysis of Particle Size Formation Utilizing PI-BPS

The DLS data further confirms what has been observed with microscopy, absorbance experiments for transitioning, and purification results. Figure 8 A-C represents the size distribution data collected on L10Flag from 10-40°C. Figure 8A shows particle size data of a un-transitioned sample of L10Flag in a neutral buffer at 10°C, which displays a small particle size in low amount. Figure 8B shows L10Flag's particle size distribution at 30°C, where it can be observed that a small shift to a larger particle size is taking place with transitioning beginning to occur. Transitioning is apparent in Figure 8C displaying L10-Flag transitioning further at 40°C, which is indicated by a further peak shift, 1.6-fold higher than 10°C, and the intensity of this particle size being nearly 1.7-fold higher than that of the un-transitioned protein in samples at 10°C and 30°C. The progression of transitioning, with temperature rising at a neutral pH, can be seen quite clearly through peak shifts and elevated intensity in Figure 8 A-C. To show the effect of highly charged ELP-fusion proteins, Figure 8 A-C is DLS data for PMPD2-L10Flag-APPIP in a neutral buffer. Here in Figure 9A it can be seen that PMPD2-L10F-APPIP particle sizes at a low temperature of 10°C, at their largest are 160 nm in size with a low intensity value of 15. When temperatures are increased, to 37°C and then 40°C in Figure 9B-C many more peaks or species are observed, with very low intensity, suggesting transitioning is being hindered and ultimately will not occur when compared to the results seen in L10Flag in a neutral buffer. This observation alludes to the fact that transitioning is occurring, but hindered, and to a very small degree (particle sizes as low as 45 nm, Figure 8C.) and in accordance with microscopy in Figure 7B where smaller particles are observed. In contrast, PMPD2-L10Flag-APPIP in a buffer at its pI, displays a large degree of transitioning (like that of unhindered L10Flag), which can be seen in Figure 10A-C when temperature is increased from 10°C to 37°C then 40°C. In Figure 10A-B, a peak shift from 122 nm to 459 nm

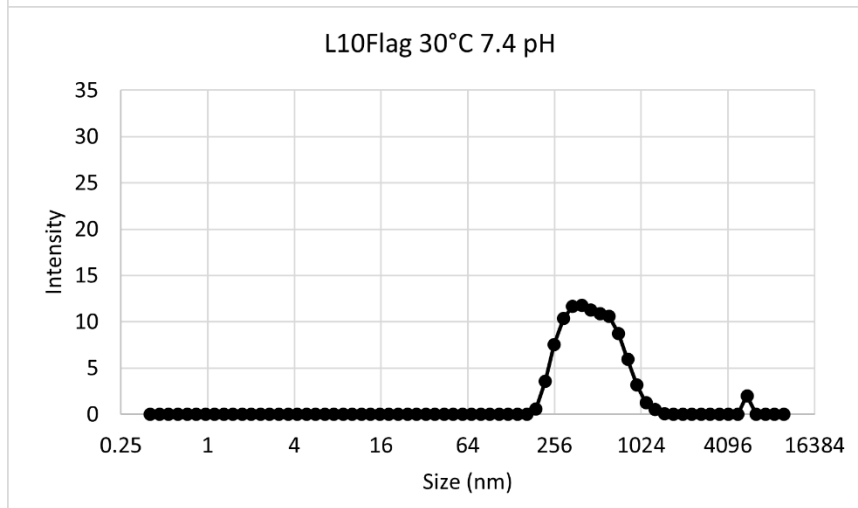
with 1.6-fold greater frequency observed when comparing PMPD2-L10Flag-APPIP at 10°C versus 37°C. Then from 37°C to 40°C, in Figure 10B-C, a further shift is observed with most particle sizes for PMPD2-L10Flag-APPIP at its pI near 531 nm with one major species. This result is like that of the unhindered L10Flag in Figure 8 A-C. The latter confirms the effect and utility of pI-BPS on ELP-based fusion molecules with highly charged ends, to both purify a practical quantity and study the transitioning impedance in an application site at a neutral pH.

Here in these DLS experiments there could be a source of error that may affect a strict reproducibility of data. The DLS machine utilized in these experiments has a internal mechanism for warming the sample to a set point temperature. Uneven heating throughout the sample will affect transitioning through a section of the sample where particle size is measured. A temperature gradient through the sample could possibly cause the sample to transition unevenly resulting in particle size differences between the similar experiments. Temperature was probed, separate from the machine's temperature measurement to aid in diminishing the amount of variance due to the possibility of uneven heating.

A.



B.



C.

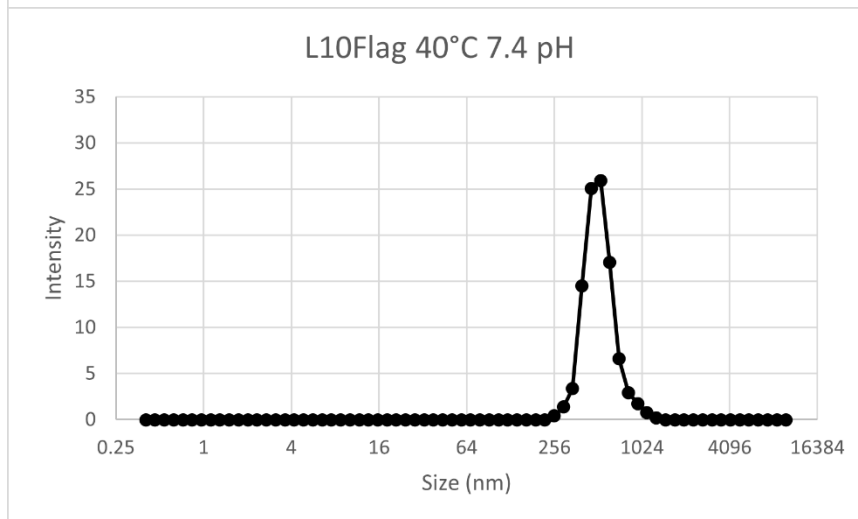
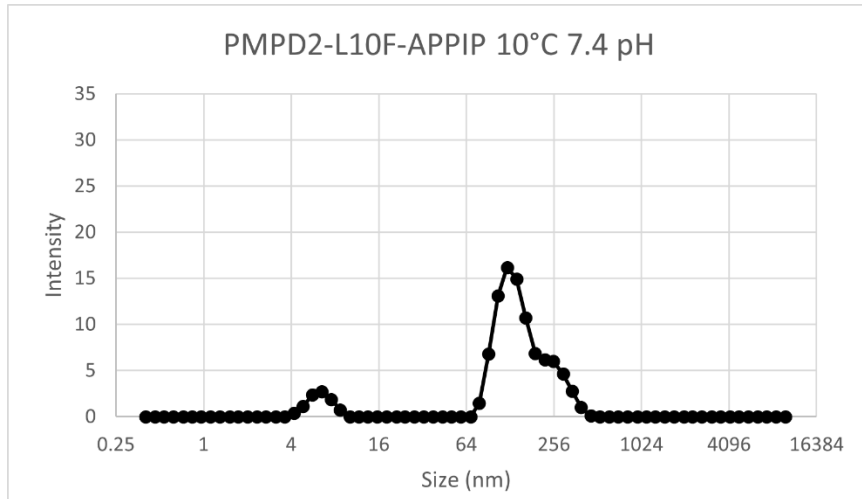
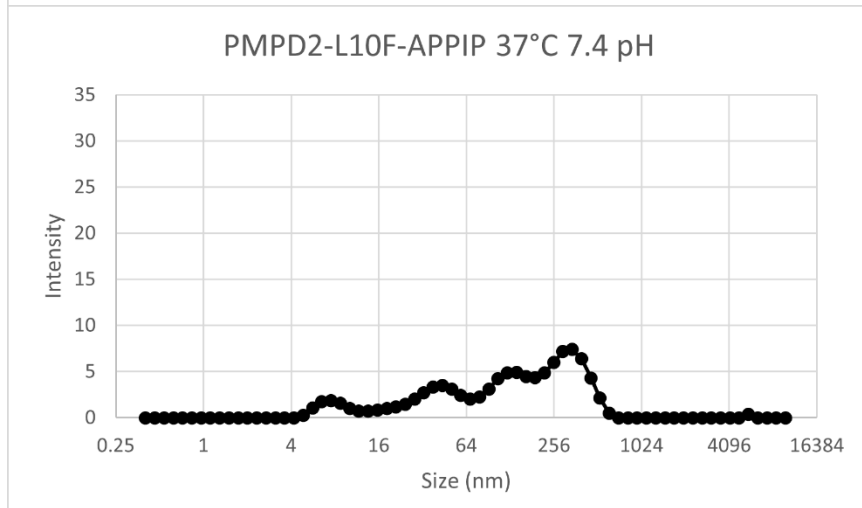


Figure 8. Dynamic Light Scattering Data for L10Flag at a 7.4 pH, from 10°C to 30°C. L10Flag at a neutral pH over temperatures A) 10°C, B) 30°C, and C) 37°C.

A.



B.



C.

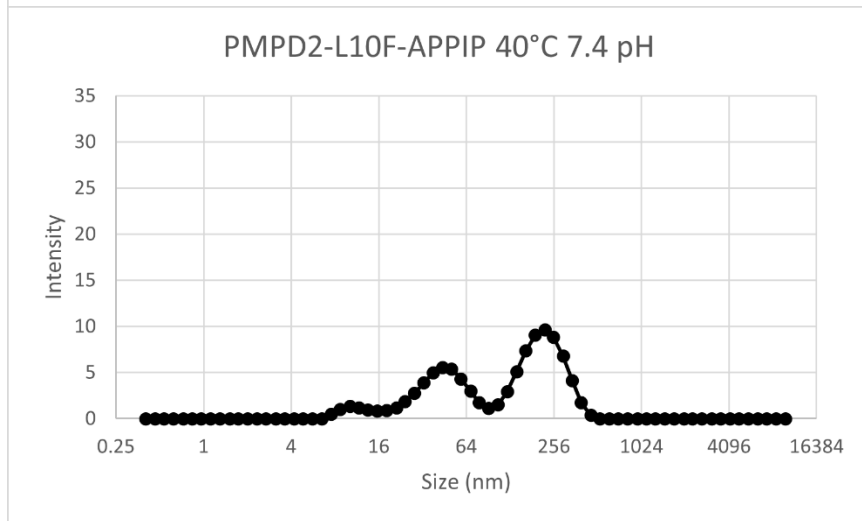
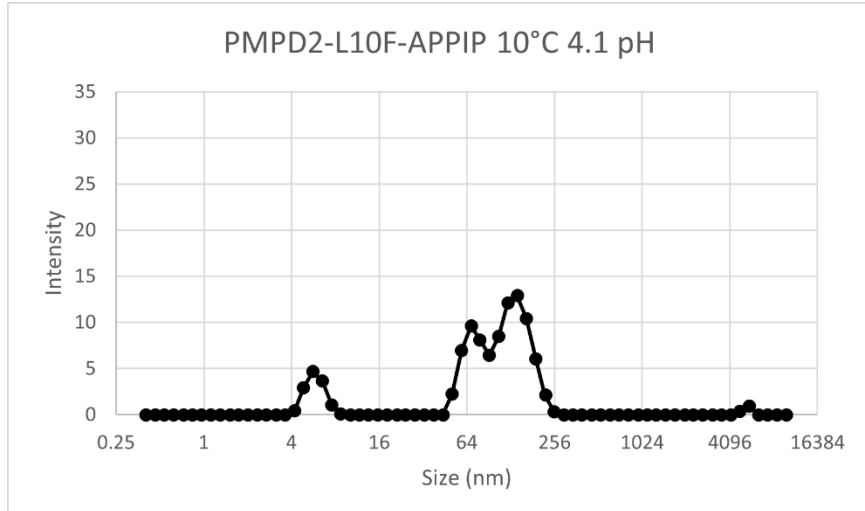
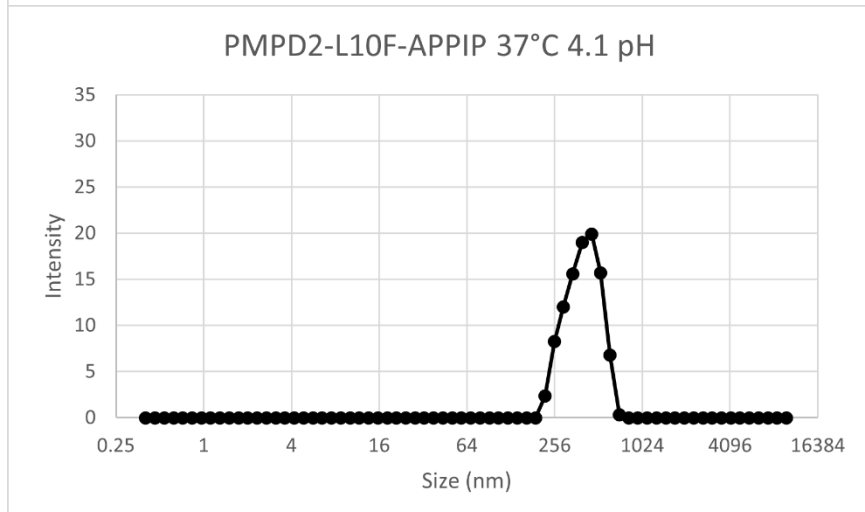


Figure 9. Dynamic Light Scattering Data for PMPD2-L10Flag-APPIP at a 7.4 pH, from 10°C to 40°C. A) PMPD2-L10Flag-APPIP a neutral pH over temperatures A) 10°C, B) 37°C, and C) 40°C.

A.



B.



C.

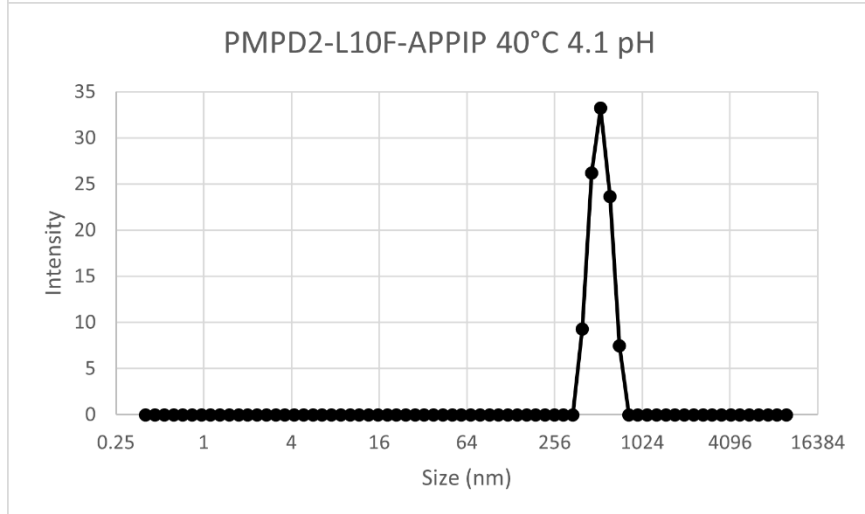


Figure 10. Dynamic Light Scattering Data for PMPD2-L10Flag-APPIP at its pI, 4.1 pH, from 10°C to 40°C. PMPD2-L10Flag-APPIP at its pI over temperatures A) 10°C, B) 37°C, and C) 40°C.

3.6 Implementation of a Matrix-Tethering ELP Fusion Protein

From the results of both the absorbance and DLS experiments for the evaluation of pH dependent phase separation, the feature of using ELP fusion proteins for sustained presence in the application site is inherently lost for fusion proteins with a high degree of hindrance of self-assembly due to charge. To implement a fail-safe method of sustaining fusion protein presence in the application site and around ECM components that require protection from proteolytic degradation, a fusion protein consisting of placental growth factor 2 (PIGF2) and a free ELP end was constructed to perform the duty of tethering PMPD2-L10Flag-APPiP. The free ELP end inherently interacts with the ELP portion of PMPD2-L10Flag-APPiP. While the PIGF2 end interacts and binds to extracellular matrix components essentially tethering the dual inhibitor to the wound bed. An experiment was ran where 1 mg/mL samples of L10Flag-PIGF2 were incubated at 42°C for 10 minutes, to transition with collagen, fibrinogen, or alone. Then each sample was centrifuged at 15,000 rpm for 5 minutes. The supernatant was discarded and the resulting pellet was resuspended in 500 µl of 1xPBS. A 6 µl sample was taken from each resulting suspension, and a total protein stain was performed on an SDS-Page gel and stained with simply safe blue (Coomassie G250), and gel pictures were taken and analyzed. Figure 11 displays a total protein staining result of the interaction of PIGF2 with fibrinogen and collagen. Here it is observed, in lanes 3-5, that L10Flag-PIGF2 has affinity for, and under centrifugation, pulls fibrinogen and collagen out of solution when heated and self-assembled. When compared to a single fusion of PMPD2-L10Flag in lanes 7-9, it is observed that L10Flag or PMPD2 may have some affinity for collagen already, but no affinity for fibrinogen. Whereas with L10Flag-PIGF2 affinity for fibrinogen is observed in lane 5.

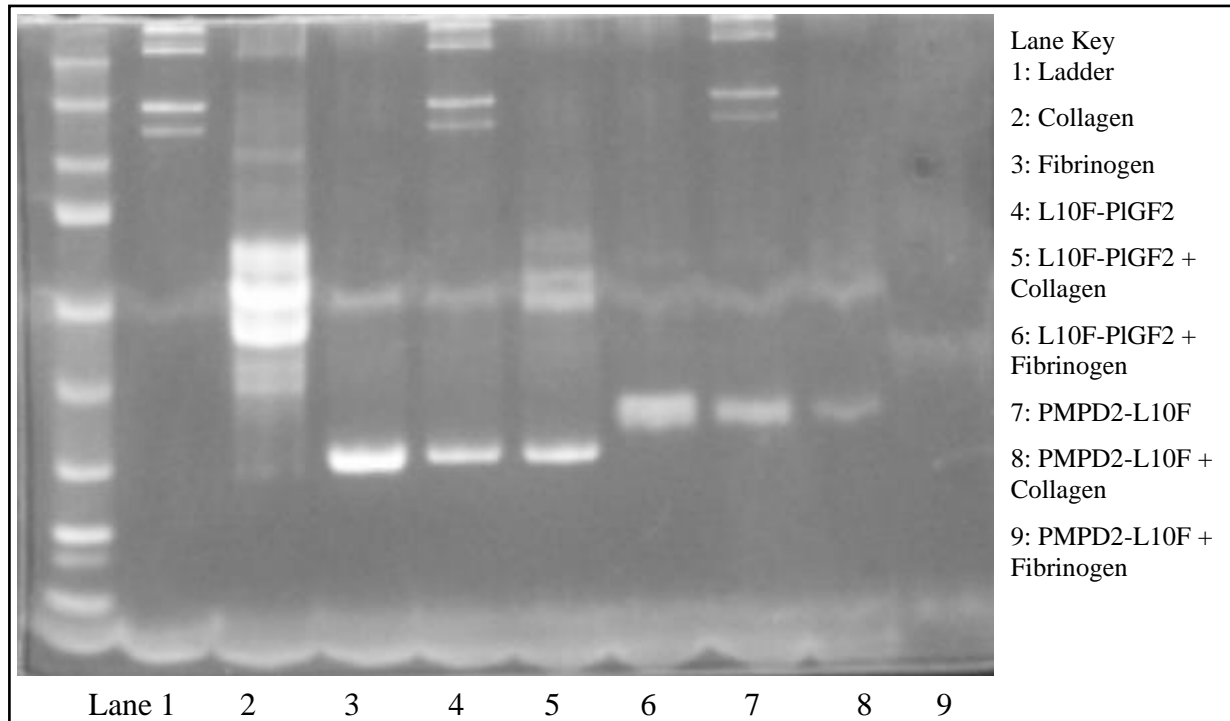


Figure 11. A Total Protein Stain of Samples of L10Flag-PIGF2 and PMPD2-L10Flag for the Evaluation of Affinity of PIGF2 for Various Matrix Proteins.

Chapter 4: Dual Inhibitory Activity of PMPD2-L10Flag-APPIP of Elastase and Matrix Metalloproteinase-2¹

PMPD2-L10Flag-APPIP was designed for dual inhibitory activity against two proteases found in high levels in chronic wounds, Neutrophil Elastase (NE) and matrix metalloproteinase-2 (MMP2). After the successful construction, synthesis, and purification of the dual protease inhibitor, assays to screen the protein's ability to block the activity of NE and MMP2 were employed. Colorimetric drug discovery kits from Enzo Life Sciences Inc. and their accompanying protocols were utilized to evaluate and determine the protein's inhibitory activity.

4.1 Methods for the Determination of PMPD2-L10Flag-APPIP's NE Inhibitory Activity

Utilizing the neutrophil elastase colorimetric drug discovery kit, the assay was performed in a 96-well plate and OD₄₁₂ read in a BioTek Synergy HT microplate reader. The two main components of this kit are neutrophil elastase and its substrate, which when cleaved creates a colorimetric product. Table 3 is a reference for the sample groups and their components in this experiment. All groups in this assay were prepared by adding and mixing all the components, besides the substrate. Then the plate was warmed to 37°C and the substrate was added to each well, besides the blank wells. All samples were ran in triplicate. The negative control contained NE, its substrate, and assay buffer. PMPD2-L10Flag-APPIP, and both single fusions, PMPD2-L10Flag and APPIP-L10Flag were tested for inhibition of NE activity at protein concentrations 5x10⁻⁷, 5x10⁻⁶, 1x10⁻⁵, and 5x10⁻⁵ µg/µl. Additionally, fusion protein blanks in triplicate were

¹ Information used in Chapter 4 has been previously published in *Biotechnology Progress*. Strauss, G. & Koria, P. Hybrid fusion protein as a dual protease inhibitor for the healing of chronic wounds. *Biotechnology Progress* **37**, e3209 (2021). Permissions included in Appendix B.

added to the plate since the experiment is ran at 37°C and protein transitioning will add to absorbance measurements. The reading was performed as a kinetic assay at a constant temperature of 37°C, over a 20-minute time interval, measuring OD₄₁₂ every minute. The absorbance from buffer and protein blanks were subtracted from the absorbance of corresponding sample groups and control during analysis to obtain true absorbance of the cleaved substrate product. The slope of the developed curves normalized to the slope of the control from collected absorbance over time data were utilized to calculate % NE inhibition employing Equation 1.

Table 3. Experiment groups of the colorimetric NE inhibition assay and their respective components

Sample Group	Components
Blank	Assay Buffer
Control	Assay Buffer + NE + Substrate
PMPD2-L1Flag-APPIP	Assay Buffer + NE +Substrate + Dual Inhibitor at various concentrations
PMPD2-L10Flag	Assay Buffer + NE +Substrate + NE Inhibitor at various concentrations
APPIP-L10Flag	Assay Buffer + NE +Substrate + MMP2 Inhibitor at various concentrations
Blanks for protein experimental groups	Assay Buffer + Inhibitor at various concentrations

$$\% \text{ Inhibition} = \left(1 - \frac{S_{\text{experimental}}}{S_{\text{neg.control}}}\right) 100\% \quad (\text{Equation 1})$$

4.2 Methods for the Determination of PMPD2-L10Flag-APPIP's MMP2 Inhibitory Activity

Utilizing the MMP2 colorimetric drug discovery kit, the assay was performed in a 96-well plate and OD₄₁₂ read in a BioTek Synergy HT microplate reader. The two main components of this kit are MMP2 and its substrate, which when cleaved creates a colorimetric product. Table 3 is a reference for the sample groups and their components in this experiment. All groups in this assay were prepared by adding and mixing all the components, besides the substrate, first. Then the plate

was warmed to 37°C and the substrate was added to each well, besides the blank wells and a kinetic absorbance reading was taken. All samples were ran in triplicate. The negative control contained MMP2, its substrate, and assay buffer. PMPD2-L10Flag-APPIP, and both single fusions, PMPD2-L10Flag and APPIP-L10Flag were tested for inhibition of MMP2 activity at protein concentrations 0.004, 0.008, 0.01, 0.05, 0.2, and 0.5 µg/µl. Furthermore, fusion protein blanks, in triplicate, were added to the plate since the experiment is ran at 37°C and protein transitioning will add to absorbance measurements. The reading was performed as a kinetic assay at a constant temperature of 37°C, over a 20-minute time interval, measuring OD₄₁₂ every minute. The absorbance from buffer and protein blanks were subtracted from the absorbance of corresponding sample groups and control during analysis to obtain true absorbance of the cleaved substrate product. The slope of the developed curves normalized to the slope of the control from collected absorbance over time data were utilized to calculate % MMP2 inhibition employing Equation 1.

Table 4. Experiment groups of the colorimetric MMP2 inhibition assay and their respective components.

Sample Group	Components
Blank	Assay Buffer
Control	Assay Buffer + MMP2 + Substrate
PMPD2-L1Flag-APPIP	Assay Buffer + MMP2 +Substrate + Dual Inhibitor at various concentrations
PMPD2-L10Flag	Assay Buffer + MMP2 +Substrate + NE Inhibitor at various concentrations
APPIP-L10Flag	Assay Buffer + MMP2 +Substrate + MMP2 Inhibitor at various concentrations
Blanks for protein experimental groups	Assay Buffer + Inhibitor at various concentrations

4.3 NE Inhibitory Activity of PMPD2-L10Flag-APPIP

Through the colorimetric kinetic assay for the evaluation of NE inhibition, inhibitory activity of PMPD2-L10Flag-APPIP was confirmed and quantified as previously reported by the author¹³. Figure 12 shows the inhibition of NE by the dual fusion protein. Utilizing the slope of the curve for each tested concentration and the negative control, Equation 1 was used to calculate % inhibition. In Figure 12 it can be observed that the dual fusion protein, when compared to the control had near zero inhibition at a concentration of $5 \times 10^{-7} \mu\text{g}/\mu\text{L}$, and full inhibition at an inhibitor concentration of $5 \times 10^{-4} \mu\text{g}/\mu\text{L}$. Through further analysis, 50% inhibitory concentration (IC₅₀) was calculated by plotting the % inhibition versus inhibitor concentration (Figure 13) and fitting the curve to produce an equation for the trend. The calculated IC₅₀ for NE by the dual inhibitor was $8.5 \times 10^{-7} \mu\text{g}/\mu\text{L}$.

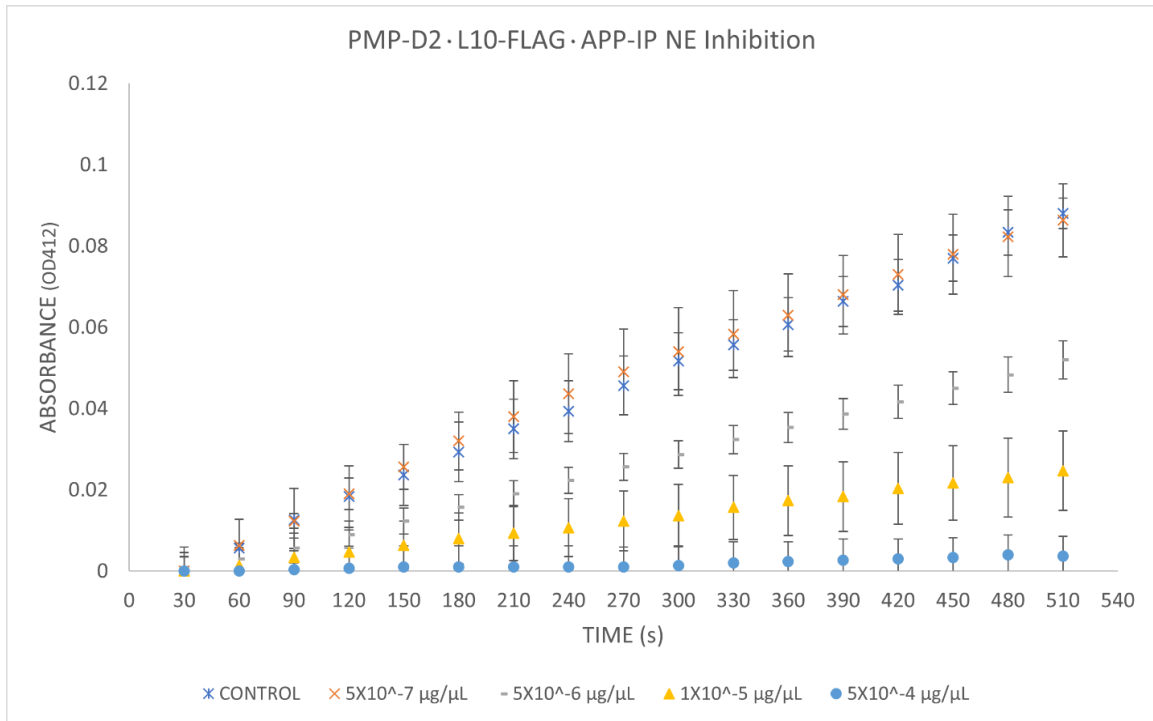


Figure 12. A Kinetic Absorbance Analysis for Concentrations of PMPD2-L10Flag-APPIP and its Inhibition of NE in the NE Colorimetric Assay.

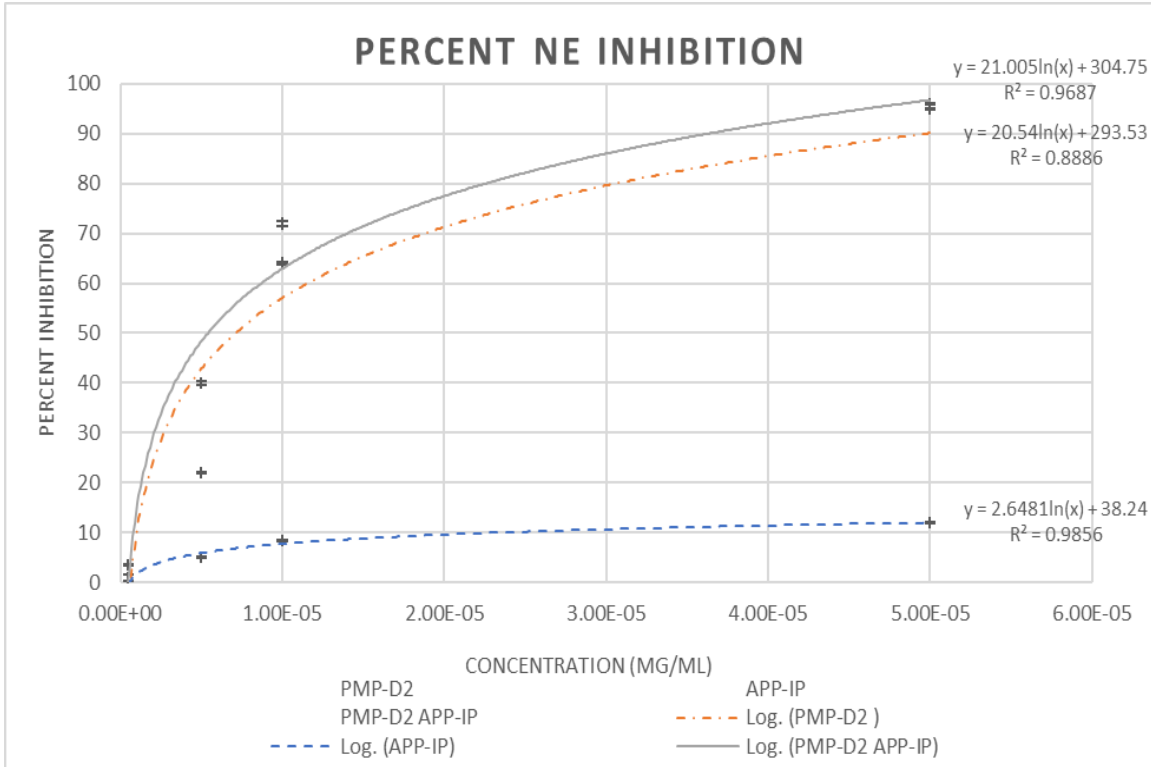


Figure 13. A Display of NE Inhibition, in % Inhibition, by the Dual Inhibitor, and the Single Fusions.

4.3.1 NE Inhibitory Activity of PMPD2-L10Flag-APPIP Compared to the Single Fusions

From the colorimetric assay for NE inhibition, single fusions, PMPD2-L10Flag and APPIP-L10Flag were tested for NE inhibition as previously reported¹³. Figure 14 A & B displays the absorbance produced throughout the kinetic assay for the single fusions and their tested concentrations for inhibition of NE cleaving the corresponding colorimetric substrate. In Figure 14A, it is observed that from a low concentration of $5 \times 10^{-5} \mu\text{g}/\mu\text{l}$ showing little inhibition when compared to the absorbance seen from the negative control. On the contrary, Figure 13B that APPIP-L10Flag is not very effective at blocking NE.

From produced percent inhibition curves and their trend line equations (Figure 13) % inhibition of each single inhibitor is displayed and utilized to calculate percent inhibition and IC

50. IC₅₀ for NE inhibition by PMPD2-L10Flag was calculated and estimated to be at a protein concentration of 7.08×10^{-6} $\mu\text{g}/\mu\text{l}$. In contrast, inhibition of NE by APPIP-L10Flag levels off at around 10% inhibition of NE at the highest tested concentration.

In comparison, PMPD2-L10Flag-APPIP and PMPD2-L10Flag had a similar IC₅₀ of 8.5×10^{-7} $\mu\text{g}/\mu\text{l}$ and 7.08×10^{-6} $\mu\text{g}/\mu\text{l}$, respectively. With an IC₅₀ for NE inhibition by the dual inhibitor being similar but lower than the single fusion, PMPD2-L10Flag, it can be concluded that the dual fusion effectively inhibits NE when compared to the single fusion PMPD2-L10Flag. However, though similar, there is nearly a 10-fold difference in IC₅₀ between the dual and single fusion for NE inhibition, with the dual inhibitor having the lower estimated IC₅₀. This can likely be attributed to the fact that the single fusion, APPIP-L10Flag, showed some quantifiable inhibitory power against NE suggesting that the dual inhibitor and each bioactive end may have the potential to act simultaneously and, in some cases, containing non-specific protease inhibition.

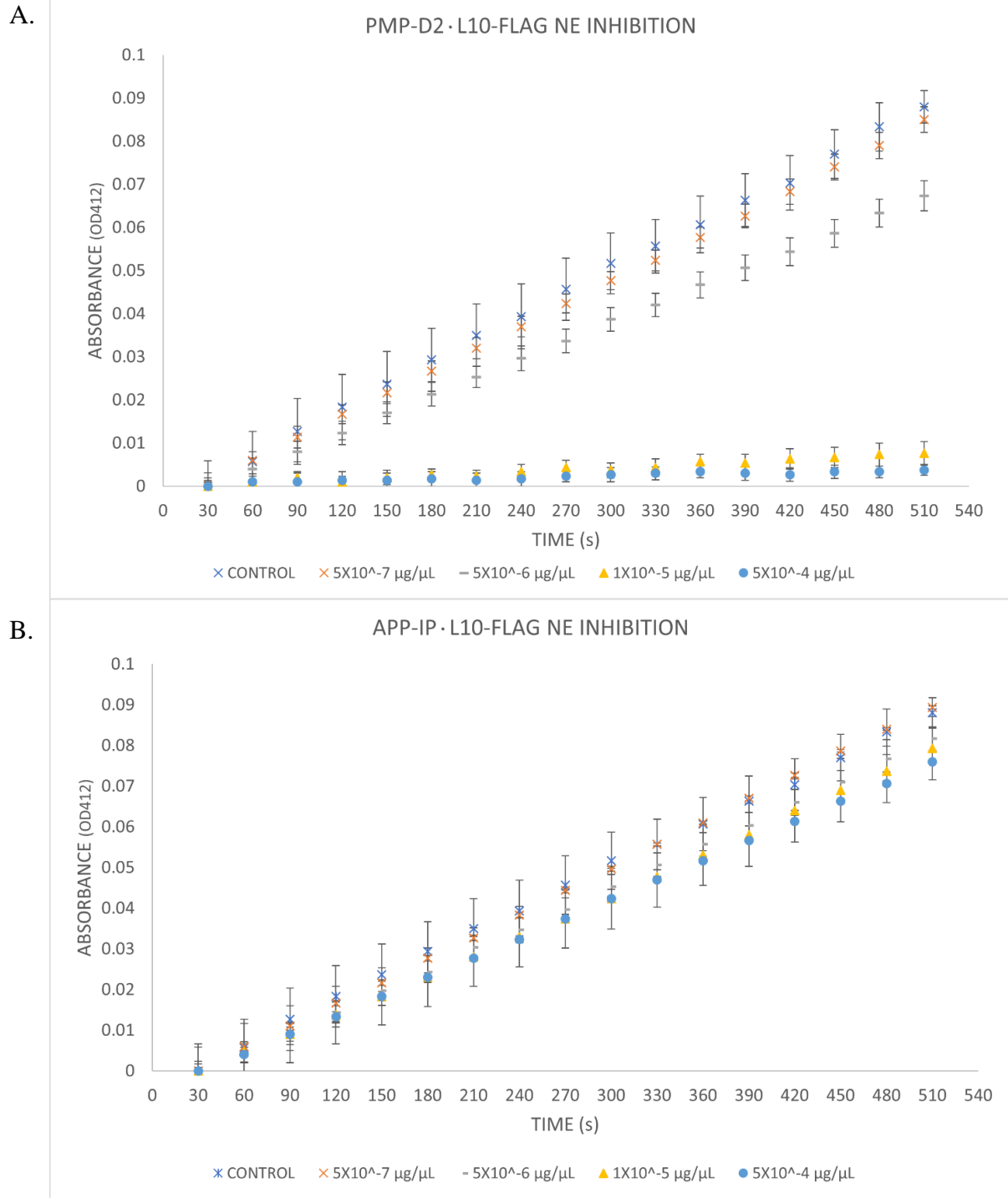


Figure 14. A Kinetic Absorbance Analysis for Concentrations of the Single Fusions, A) PMPD2-L10Flag and B) L10Flag-APP-IP and Their Inhibition of NE in the NE Colorimetric Assay.

4.4 MMP2 Inhibitory Activity of PMPD2-L10Flag-APPIP

From the colorimetric kinetic assay for the quantification of MMP2 inhibition, inhibitory activity of PMPD2-L10Flag-APPIP was confirmed as previously reported by the author¹³. Figure 15 shows the inhibition of MMP2 by the dual fusion protein. Utilizing the slope of the curve for each tested concentration and the negative control, Equation 1 was used to calculate % MMP2 inhibition. Here in Figure 15 it can be observed that the dual fusion protein, when compared to the control had near zero inhibition at the lowest tested concentration of 0.004 $\mu\text{g}/\mu\text{l}$, and near full inhibition at an inhibitor concentration of 0.5 $\mu\text{g}/\mu\text{l}$ where it is seen that the slope of the absorbance over time is close to 0. Through further analysis 50% inhibitory concentration (IC₅₀) was calculated by plotting the % inhibition versus inhibitor concentration (Figure 16) and fitting the curve to produce an equation for the trend. The calculated IC₅₀ for MMP2, inhibited by the dual inhibitor was 0.04 $\mu\text{g}/\mu\text{l}$.

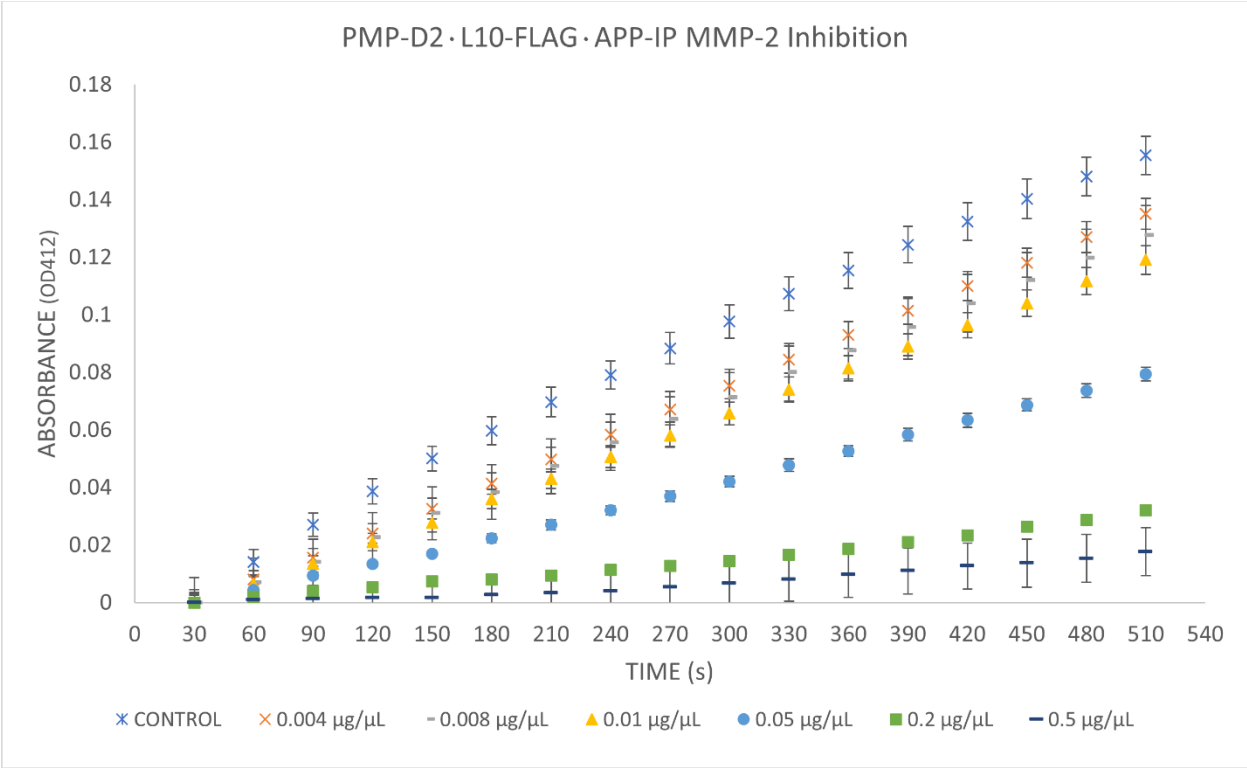


Figure 15. A Kinetic Absorbance Analysis for Concentrations of PMPD2-L10Flag-APPIP and its Inhibition of MMP2 in the MMP2 Colorimetric Assay.

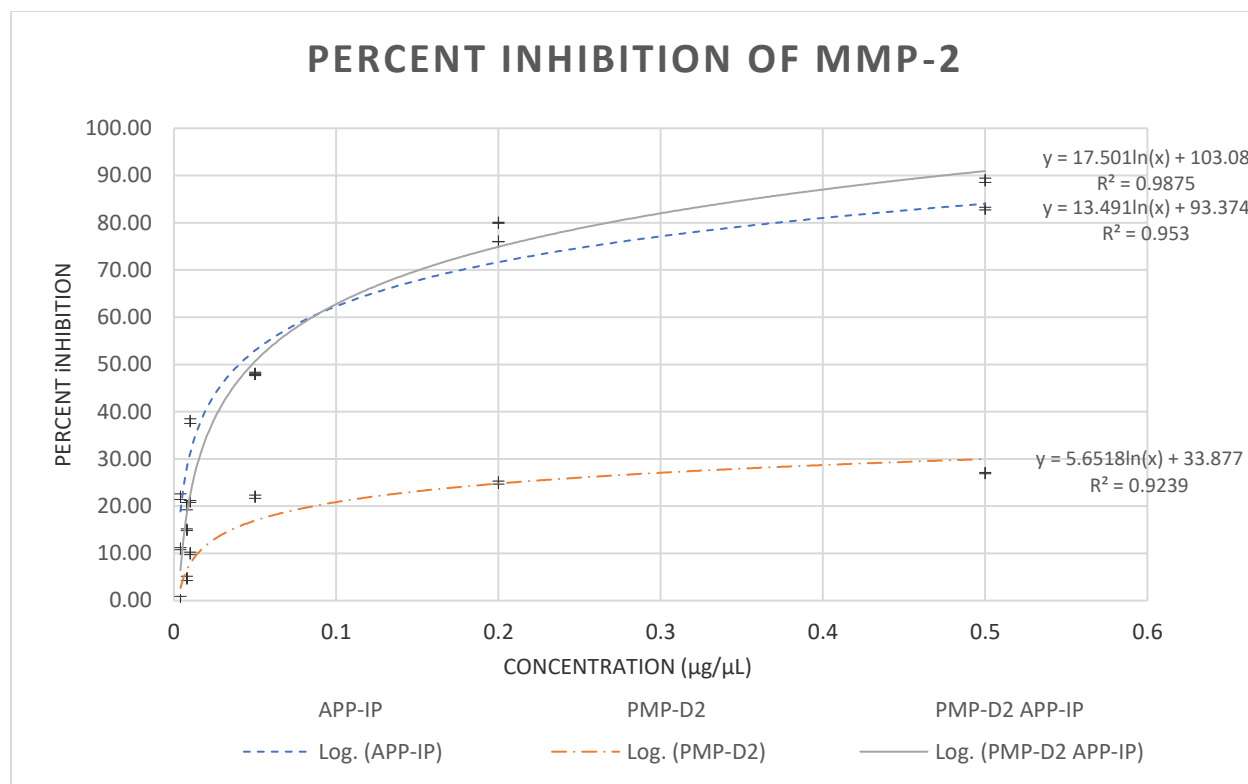


Figure 16. A Display of MMP2 Inhibition, in % Inhibition, by the Dual Inhibitor, and the Single Fusions.

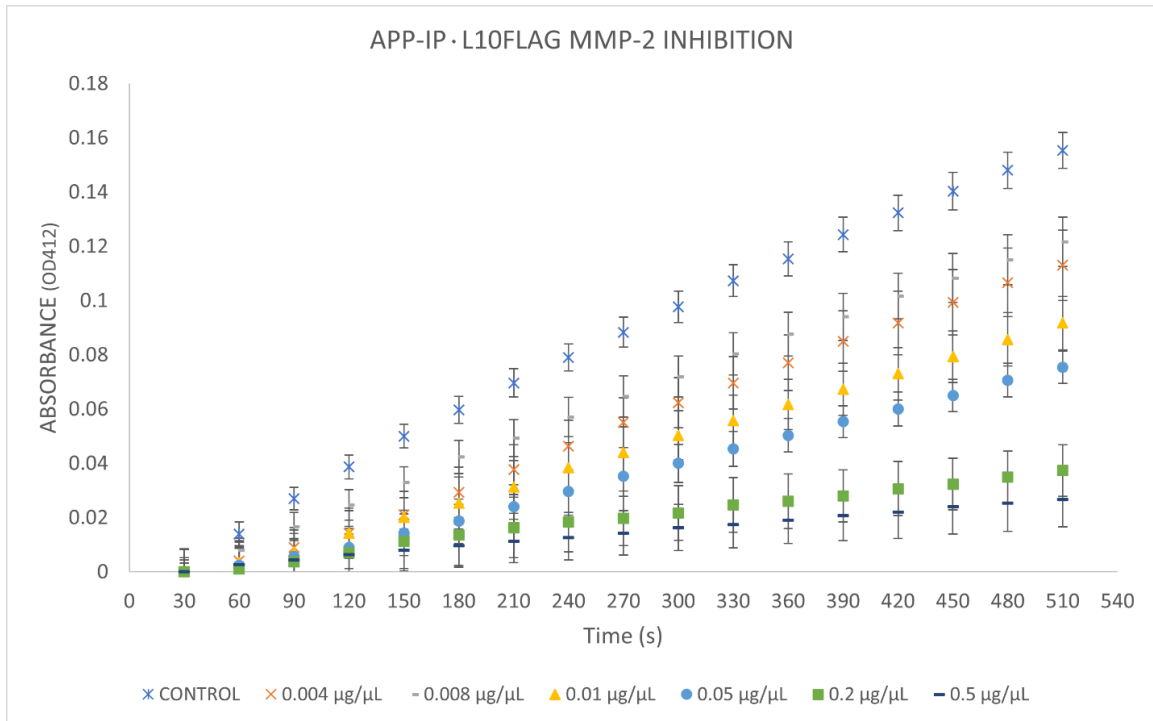
4.4.1 MMP2 Inhibitory Activity of PMPD2-L10Flag-APPIP Compared to the Single Fusions

Gained from the colorimetric assay for MMP2 inhibition, single fusions, PMPD2-L10Flag and APPIP-L10Flag were tested for MMP2 inhibition as previously reported¹³. Figure 17 A & B displays the absorbance produced throughout the kinetic assay for the single fusions and their tested concentrations for inhibition of NE cleaving the corresponding colorimetric substrate. In Figure 17A, it is observed that from a low APPIP-L10Flag concentration of $5 \times 10^{-5} \mu\text{g}/\mu\text{l}$ showing little inhibition, like the negative control, to a highest tested concentration of $0.5 \mu\text{g}/\mu\text{l}$ with near complete inhibition. On the contrary, in Figure 17B, PMPD2-L10Flag is not nearly as effective at blocking MMP2 as the single fusion, APPIP-L10Flag.

From produced percent inhibition curves and their trend line equations (Figure 15) % inhibition of each single inhibitor is displayed and utilized to calculate percent inhibition and IC₅₀. IC₅₀ for MMP2 inhibition by APPIP-L10Flag was calculated and estimated to be at a protein concentration of 0.05 µg/µl. In contrast, inhibition of NE by APPIP-L10Flag levels off at around 20% inhibition of NE at the highest tested concentration.

In comparison, PMPD2-L10Flag-APPIP and APPIP-L10Flag had a similar IC₅₀ of 0.04 µg/µl and 0.05 µg/µl, respectively. This result concludes that the dual fusion made to create PMPD2-L10Flag-APPIP does not negatively affect the inhibitory capabilities in the application of this dual protease inhibitor when compared to a single fused inhibitor, APPIP-L10Flag, for MMP2 inhibition.

A.



B.

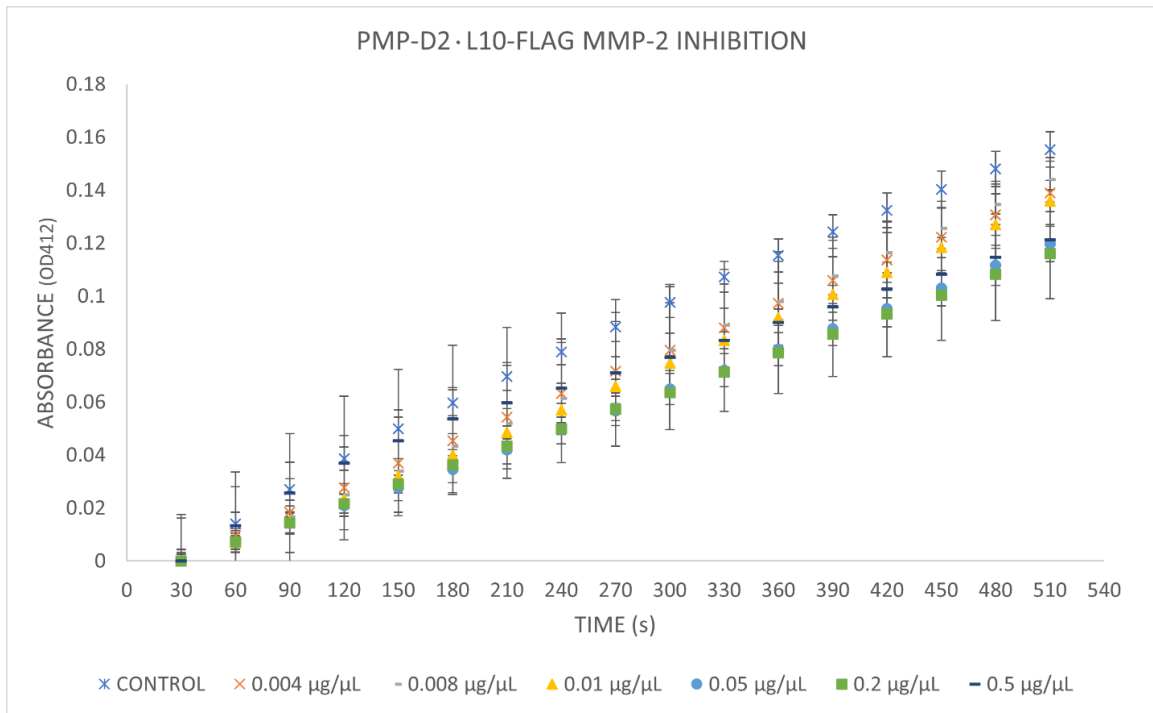


Figure 17. A Kinetic Absorbance Analysis for Concentrations of the Single Fusions, A) PMPD2-L10Flag and B) L10Flag-APPIP and Their Inhibition of MMP2 in the MMP2 Colorimetric Assay.

4.5 Dual and Simultaneous Inhibition of NE and MMP2

Additional to the standard screening for PMPD2-L10Flag-APPIP inhibition of NE and MMP2, an experiment was run to evaluate the protein's ability to bind and block NE and MMP2 concurrently. The experiment was run in accordance with the MMP2 and NE colorimetric drug discovery kits from Enzo Life Sciences Inc. However, this experiment was run in both the presence of NE and MMP2, rather than separate experiments as previously described. In this case two controls were made, one that just contained assay buffer, NE, and substrate, and the other with assay buffer, NE, MMP2, and substrate. Two experimental groups were formed: the first with assay buffer, NE, substrate, and the dual inhibitor; while the other with assay, buffer, NE, MMP2, substrate, and the dual inhibitor. Both experimental groups contained the dual inhibitor at a concentration of 0.05 $\mu\text{g}/\mu\text{l}$. Figure 18 displays clearly that in the negative control containing just 1 protease, NE, chewed up the substrate as indicated by the slope of the absorbance curve. The negative control that contained two proteases, NE and MMP2, further chewed up the existing substrate elevating the slope even further. Also in Figure 18, are the results of the experimental groups with the dual inhibitor. Both the experimental groups showed inhibition to a similar level as indicated by similar slopes of their respective absorbance curves in comparison to the controls. This result confirms PMPD2-L10Flag-APPIP's ability to block both NE and MMP simultaneously and effectively.

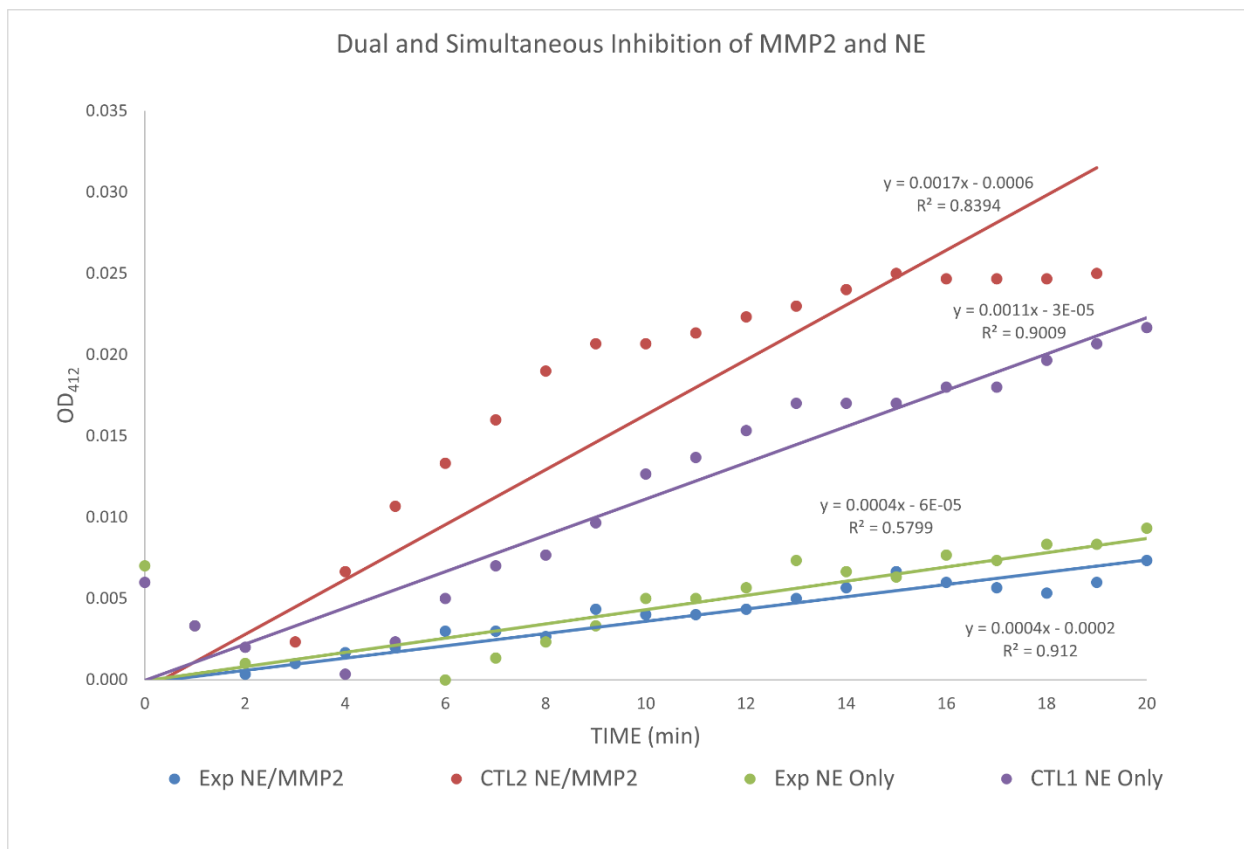


Figure 18. The Simultaneous Activity of Each Bioactive End of PMPD2-L10Flag-APPIP in a Kinetic Inhibition Assay Containing MMP2 and NE.

4.6 Statistics and Sources of Error in the Inhibition Experiments

Standard deviation of the average absorbance is applied to the graphs of inhibition. Possible sources of error are rooted in the transitioning properties of the ELP-based inhibitors. Since the ELP-fusion proteins may transition at the 37°C experiment parameter, ELP-fusion protein blank samples were added to the experiment to account for transitioning that may add to the absorbance of the colorimetric measurement. This could be a possible source of error propagation as the degree of transitioning is highly dependent on the accuracy of inhibitor concentration in both the experimental and blank wells.

Chapter 5: Mesenchymal Stem Cells and Their Ability to Condition Media Into a Potent Proliferation Inducing Cocktail

Human Mesenchymal Stem Cells (MSCs) have been widely used in numerous ways to treat a variety of diseases. Most notably, mesenchymal stem cells harvested from the umbilical cord, bone, amniotic fluid, and adipose tissue²³ have commonly been used as a cellular-based therapy for the treatment of diseases that cause tissue degeneration or debilitating tissue damage. Their attractiveness for cellular therapy is wide spread, where they are utilized as a whole cell for their multi- and pluripotency that in theory lend them useful in application in the body to seed new cells of the damaged tissue type²³⁻²⁵. Furthermore, their application has gone as far as to suggest a usefulness of the products contained inside of extracellular vesicles produced and secreted by MSC's²⁵. With many application styles of MSCs and their products they produce, the commonality in their use is the pursuit of promoting tissue healing. Whether that is through the delivery of the pluripotent cell with the capacity for differentiation²³⁻²⁵, the immunomodulatory and anti-inflammatory qualities of MSCs^{23,26}, or for the various regenerative biproducts that MSCs produce to influence cellular migration, growth, and protein deposition for complete tissue repair²².

Regarding cellular biproducts created by MSCs, this has been previously studied to some degree where it was determined that conditioning biproducts of MSCs include some very prominent wound healing peptides such as EGF, TGF α , TGF β 1, VEGF, FGF2, as well as many immunosuppressing and modulating proteins²². Wound healing and tissue regeneration rely on a lot of these growth factors and peptides in natural tissue healing processes. Vascular endothelial growth factor (VEGF) is important to stimulate remodeling processes like cellular migration and

proliferation²⁷. Endothelial growth factor (EGF) is important for stimulating re-epithelialization of a wound, while transforming growth factors such as TGFb1 and TGFa aid in re-epithelialization but also in matrix formation and remodeling of the wound¹⁷ which is important for regaining structural integrity in newly healed or formed tissue. Similarly, Fibroblast Growth Factor 2 (FGF 2) helps aid in the remodeling and matrix formation process¹⁷. Growth factors such as EGF, TGFa, TGFb1, FGF2, and VEGF have all been found to increase in levels in a naturally healing acute wound with no therapeutic intervention, but have been seen in decreased levels in chronic wounds¹⁷.

Here it is proposed that due to current knowledge of chronic wounds and that there are growth factor species whose levels can be correlated with an acute healing wound versus a chronic wound¹⁷, it is advantageous to replace the growth factors that are seen in suppressed levels in chronic wounds to move the wound to closure. As previously drawn, there is a correlation, between the proteins needed in wound healing, and those that have been found to be produced by mesenchymal stem cells. Therefore, a great candidate for proliferation inducing therapies to aid in the remodeling of hard-to-heal or chronic wounds, is media conditioned by stem cells, which include proteins that are essential to cellular migration, proliferation, and remodeling of the wounded tissue. A protein cocktail, from the conditioning of media, by mesenchymal stem cells can easily be mixed with other protein-based therapeutics, such as the protease inhibitor described here to create a self-protecting therapeutic to aid in the downregulation of protein destroying proteases found in high levels in chronic wounds, while delivering and protecting present growth factors necessary for tissue regeneration of the skin.

5.1 Culturing of Mesenchymal Stem Cells

Human umbilical cord derived mesenchymal stem cells (um-MSCs) were obtained from ATCC and plated in a 100 mm dish. The culture was expanded to confluency in 10 mL of basal stem cell culture media, MesenPRO RS (GibcoTM), and supplemented with 2% stem-cell qualified FBS. The cells were maintained at 37°C and 5% CO₂. The MSCs were passed when 80% confluency was reached, utilizing 0.25 trypsin-EDTA, and sub-cultured in 100 mm dishes. It was observed that um-MSC subcultures would expand at a steady rate out to 5 to 6 passages (changing media every 2 days, reaching confluency and passing every 5 to 7 days). Upon media collection and media replacement, 2 mL of media from the last 48-hour incubation was reserved in the dish, and 8 mL of new media was added. Around passage 5, proliferation would slow down and the MSCs would stay at around a 70-80% confluency, without cell death if maintained by the described media replacement every 48-hours.

5.1.1 Harvesting Um-MSC Conditioned Media

Throughout the expansion process of these um-MSC's, during media replacement (every 48 hours) the media was collected from a MSC culture that was near 70 to 80% confluency and stored to be screened for proliferative effects *in vitro*. However, it was observed that when the um-MSCs, themselves, slowed down in proliferation they still maintained healthy cellular morphology and attachment. So, a sub-culture of passage 5 um-MSC's were maintained in this state where the MSCs were live and healthy, but not dividing at a steady rate wouldn't lead to another sub-culture. Every 48 hours the media was replaced, and the old media collected and stored at -20°C. In some cases, these slow growing cultures could be maintained for weeks to well over a month while collecting a potent conditioned media, without death of the MSCs.

5.1.2 Processing the Um-MSC Conditioned Media

Before use of the MSC conditioned media, all samples to be screened were thawed and filtered with a 0.22 μm filter to result in an acellular product, just containing free proteins and soluble small molecules that will remain after filtration. In some cases, the conditioned media was applied in vitro as a liquid to test for its ability to cause proliferation, while in other cases it was freeze dried through lyophilization and applied as a dry product. Additionally, in some experiments, filter paper was soaked in conditioned media, frozen, and then lyophilized to embed the conditioning products within a solid medium.

5.1.3 Verification of Um-MSCs

Flow cytometry was employed to verify the mesenchymal stem cells using criteria of cell surface markers to characterize human derived MSCs. MSCs are characterized as positive for CD73, CD90, and CD105 cell surface markers²⁸. Furthermore, MSC characterization guidelines require them to be negative for the cell surface markers CD14, CD34, and CD45²⁸. Conjugated antibodies for CD73, CD90, and CD105 were obtained and to be utilized with florescent flow cytometry channels for excitation and emission of FITC, thy-1 phycoerythrin, and allophycocyanin respectively. While the negative markers were identified with human Alexa Flour 405 conjugated human antibodies, the same channel as DAPI. DAPI was used in a fully stained sample of MSCs to evaluate viability. A fully stained sample without DAPI added was evaluated for negative marker expression. All negative and positive antibodies were added to a dilute sample of Um- MSCs and analyzed for positive and negative marker expression. To acquire negative marker expression a comparison must be made between a fully-stained sample with DAPI, and a fully stained without the addition of DAPI. Figure 19 displays the progression of analysis and identification of um- MSC's through the staining of the positive markers CD73, CD90, and CD105

with differing conjugates, as well as DAPI to determine viability of the sample. As it can be seen from the data reported in Figure 19, cells containing the CD73 positive marker have been identified and exist on the surface of 100% of the live, parent population that expresses both CD90 and 105, with 84% of all live cells detected are positive for all three markers. Figure 20 displays the flow cytometry results of a fully stained sample without DAPI, but still acquiring measurements utilizing the DAPI channel, for the isolation of cells that may present negative markers disqualifying them as MSCs. In Figure 20 it is observed that there is no negative marker expression. These results validate the use of these cells as MSCs for conditioning of media. Furthermore, this sample contained a 74% viability post isolation and staining for flow cytometry.

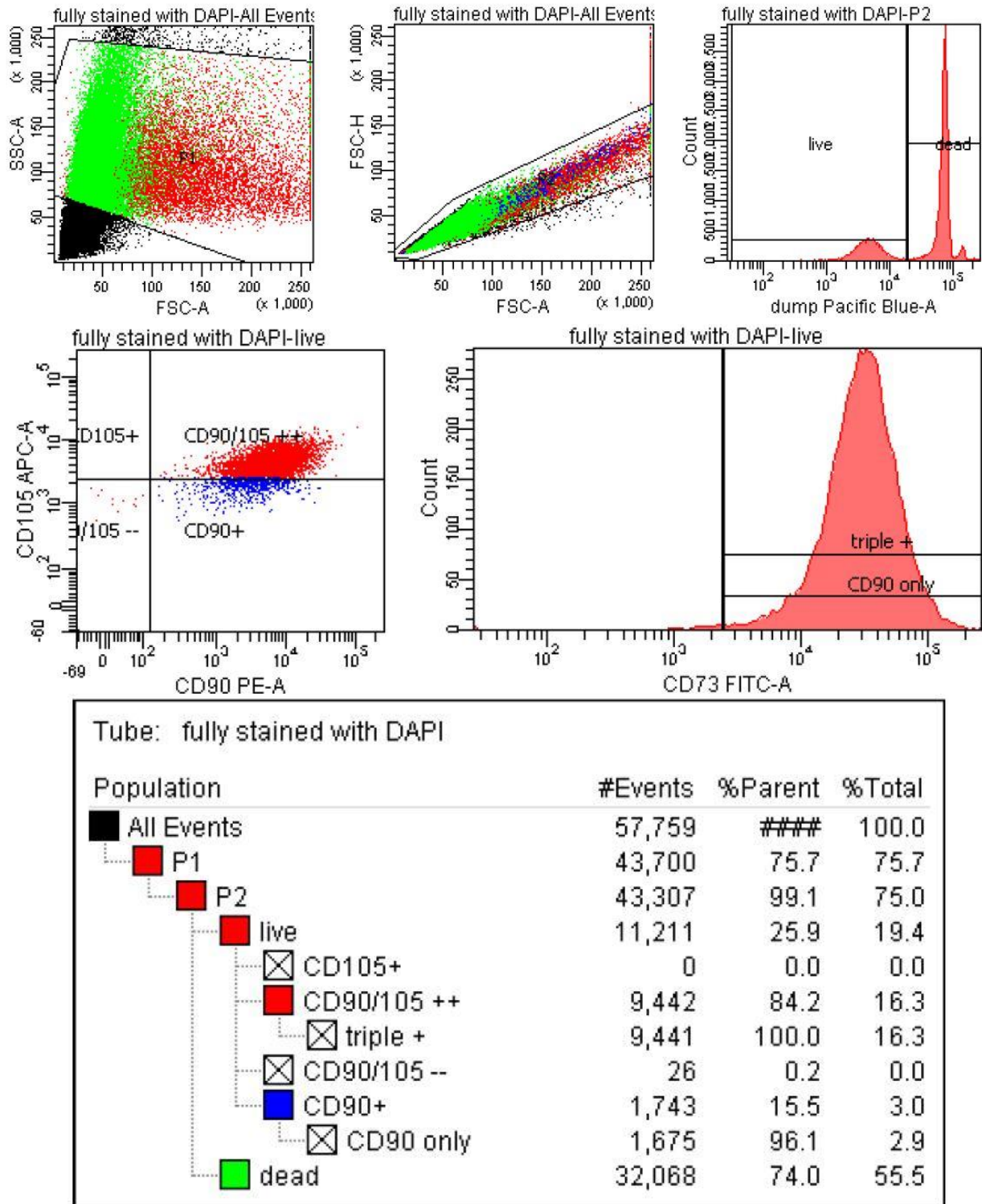


Figure 19. Flow Cytometry Results of Um-MSC's Targeting the Expression of Each Positive Marker for Mesenchymal Stem Cell Determination.

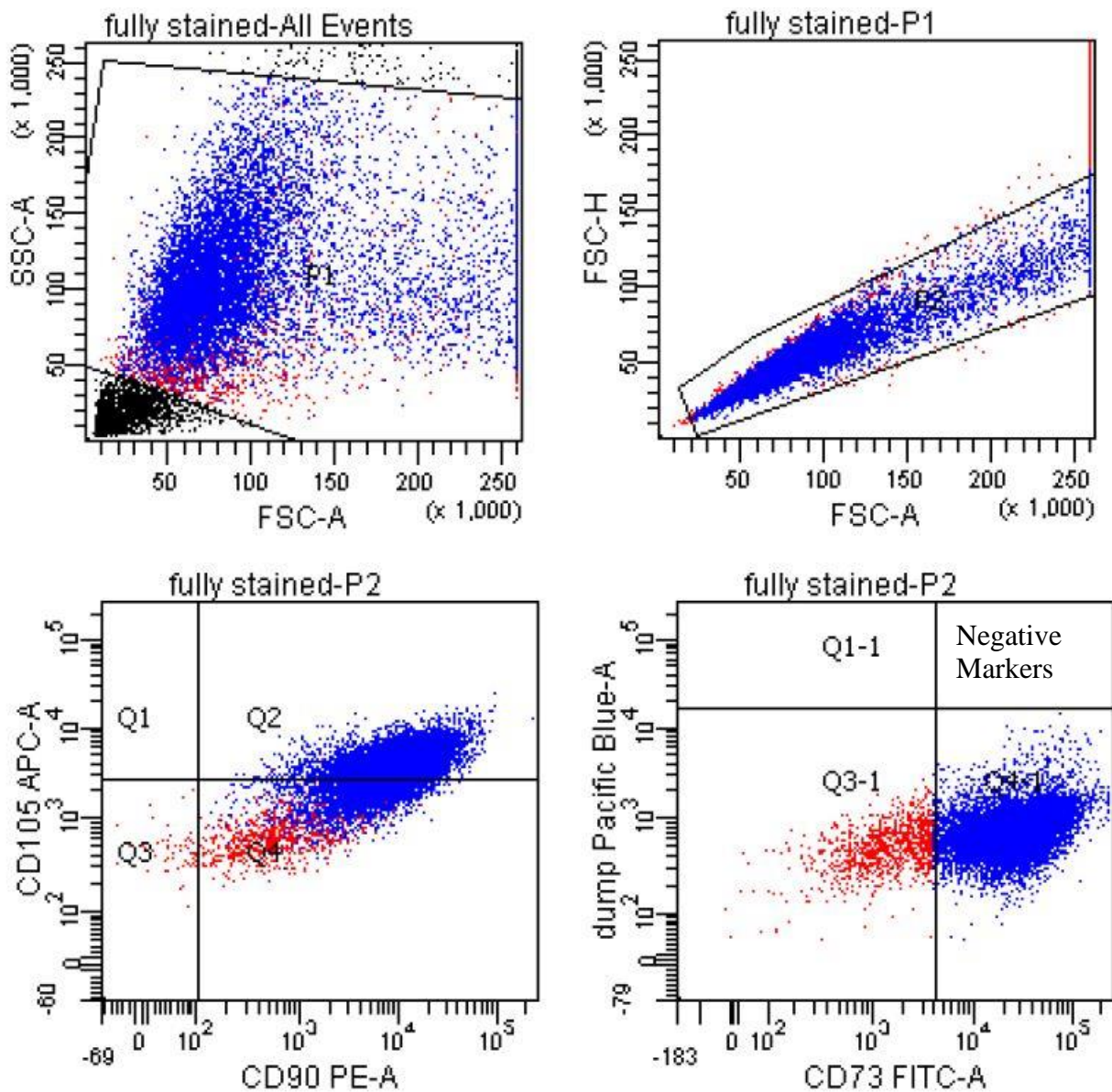


Figure 20. Flow Cytometry Results of Fully Stained Cells Without DAPI to Determine the Degree of Negative Marker Expression.

5.2 Screening Um-MSC Conditioned Media for Inducing Cellular Proliferation

C2C12, a mouse muscle myogenic cell line from ATCC was obtained. C2C12 cells have shown quick responsiveness to growth factor induced proliferation and growth as previously used by this laboratory²⁹. C2C12 cells were removed from liquid nitrogen storage and seeded at a density of 10^6 cells per 100 mm dish. The cells were maintained in DMEM 10% FBS supplemented with 1% antibiotic-antimycotic (AA) at 37°C and 5% CO₂. The C2C12 cells expanded to 80% confluency were then passed to 24-well plates, at a seeding density of 5×10^4 cells per well, for treatment with MSC conditioned media product.

5.2.1 Proliferation Experiments Utilizing C2C12 Cells in a Serum-Free Environment

C2C12 cells were plated at a seeding density of 5×10^4 cells per well and incubated at standard culturing conditions (37°C and 5% CO₂) over night for attachment. After attachment, the cells in each well were washed three time in 1xPBS, and after the last wash, serum-free DMEM 1% AA was added to each control (n=12) and experimental well (n=12). Then, 0.2 mL of serum-free MesenPRO RS was added to each control well for a final volume of 0.4 mL. MSC conditioned media (200 µl) was then added to each experimental well (n=12), for each conditioned media sample) on the 24-well plate for a total and final volume of 0.4 mL in each well. The assay plate with control wells and treatment wells was then incubated under standard cell culture conditions for 72 hours.

Following the incubation period, the cells were washed three times in 1xPBS and after the last wash 200 µl of deionized water was added to each assay well. Then, a Hoechst assay was employed by utilizing three freeze-thaw procedures to lyse the cells. A 100 µl sample of the lysate was taken from each well and transferred to a corresponding well on a 96-well, round bottom, assay plate. Hoechst 33342, at a working concentration of 0.002 mg/mL was added 1:1 with each

lysate sample, with a final volume of 200 μ l in each well to be analyzed on the 96-well plate. The assay was then read, Ex/Em 360/460, after a 30 second shaking procedure on a BioTek Synergy HT microplate reader. The resulting data was blanked and analyzed by comparing the degree of fluorescence, which corresponds to the number of cells in each well, compared to that of the control wells. The average fluorescent results of the conditioned media treatment wells were divided by the average fluorescence of the control wells, and multiplied by 100%, to normalize the results to that of the control, and display % growth.

5.2.2 Proliferation Experiments Utilizing C2C12 Cells Treated with MSC-CM and NE

The proliferation experiment using um-MSC conditioned media to induce proliferation, was employed again, but with levels of protease added to the treatment to visualize the affect proteases have on the conditioned media protein products that will fall victim to the inherent threat of proteolytic degradation seen in hard-to-heal wounds. After plating C2C12 cells in a 24-well plate and allowing for overnight attachment in standard cell culture conditions, all wells were washed three times in 1xPBS. Immediately after aspirating the last washing procedure, serum free DMEM with 1% AA was added to each control and experimental well. Utilizing the same conditioned media sample, 0.2 mL of processed conditioned media was added to each treatment well for a total final volume of 0.4 mL. While the control wells (n=6) received 0.2 mL of serum-free MesenPRO RS media. One group of conditioned media treated wells were left unexposed to protease, while other well groups (n=6) received various concentrations of elastase with the largest concentration of elastase being 200 mU/mL, a clinically relevant level of protease¹⁸, to see the true degrading affect that protease levels have on the potential use of conditioned media products in chronic or hard-to-heal wounds. The elastase concentrations tested were 0.02, 0.2, 2, 20, and 200 mU/mL.

After treatment, the 24-well plate was incubated under standard cell culture conditions for 72-hours and then a Hoechst assay was utilized to analyze the proliferative effects of the conditioned media in the presence of protease. The Hoechst assay was performed and analyzed in accordance with the protocol described in section 5.2.1.

5.3 Induction of Proliferation of C2C12 Cells Treated with Um-MSC Conditioned Media With or Without the Presence of Proteases

Umbilical cord derived MSC conditioned media obtained from the harvesting of the used media from MSC's in section 5.1.1 was used to induce proliferation in C2C12 mouse myogenic cells *in vitro*. Figure 21 displays the experimentation with various samples from different collections of um-MSC conditioned media. Here, it is observed that samples such as MSC 1 and MSC 4 induced a 4.8-fold increase in cellular proliferation when compared to the untreated control. MSC 3 in Figure 21, caused the least amount of proliferation, but was still 3.6-fold higher proliferation than that of the untreated control.

Figure 22 displays the results of a proliferation assay with C2C12 cells treated with conditioned media, and various concentrations of NE. Um-MSC conditioned media sample MSC 3 from the experiment results reported in Figure 21 was the sample used for treatment with the various concentrations of NE and showed similar induction of proliferation, in Figure 22 when NE=0 mU/mL. This is important to note as it expresses the consistency in capturing proliferation induction using this assay. Though, in Figure 22 when analyzing the effect of NE on conditioned media treatments, it is seen that at 200 mU/mL of NE there is a significant decrease in C2C12 proliferation, but as the concentration of NE is lessened, proliferation steadily increases back to the degree of proliferation observed in the MSC conditioned media treatment with no NE. In Figure 22, there is a 1.6, 1.14, and 1.1-fold decrease in proliferation, for 200, 20 and 2 mU/mL

concentrations of NE respectively, compared to cells that were treated with just MSC conditioned media. At an NE concentration of 0.2 and 0.02 mU/mL it is observed that proliferation is that of the C2C12 cells that were treated with just MSC conditioned media, no inhibitor. The latter result drives the importance in combining the dual protease inhibitor with um-MSC conditioned media

Figure 23 displays the proliferation results when utilizing MSC conditioned media in dry forms *in vitro*. As it is observed in Figure 23, all dry processed um-MSC conditioned media caused proliferation over that of the untreated control. The MSC conditioned media embedded filter paper had a 1.44-fold increase in proliferation over the degree of proliferation of untreated control. While lyophilized products that were dialyzed, or not, and used in powder form showed a 2.98 and 3.50-fold increase in proliferation. These results align closely with liquid-based treatments, except for the filter paper embedding of MSC conditioned powder and the deviation here is due to the fact that there is volume limitations for embedding the powder within a thin piece of material.

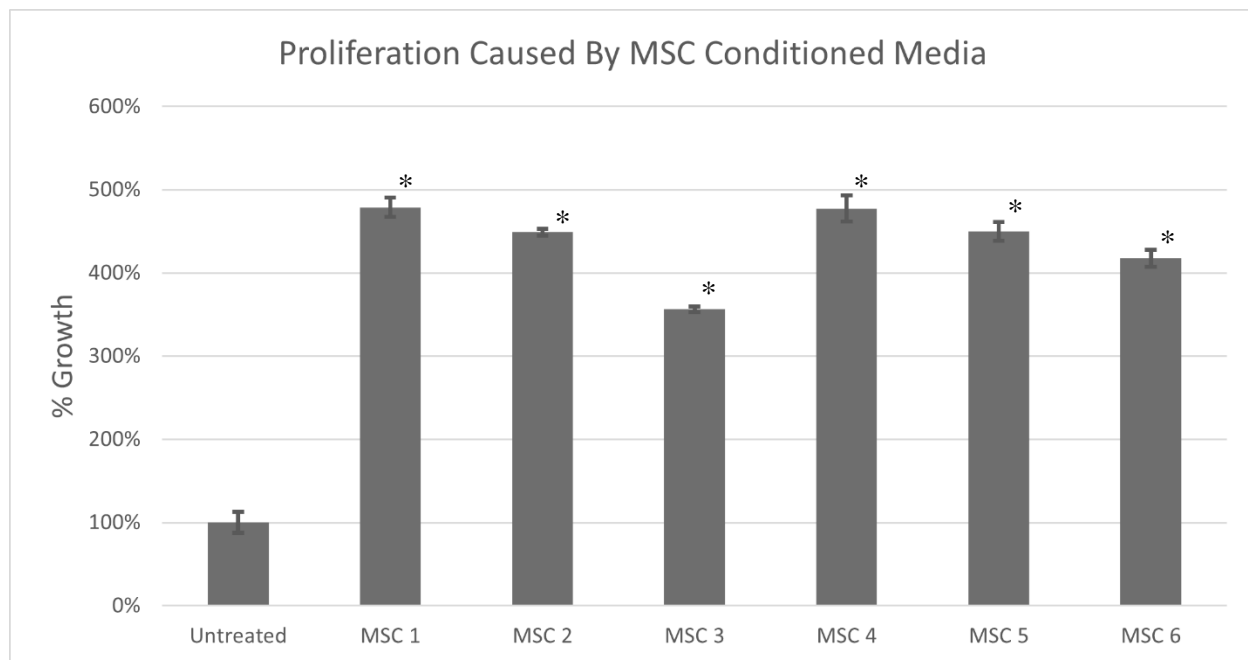


Figure 21. The Proliferation of C2C12 Cells Treated with Various Collections of Um-MSC Conditioned Media.*Statistically significant compared to an untreated control with $p \leq 0.05$ and $F_{crit} \leq F$.

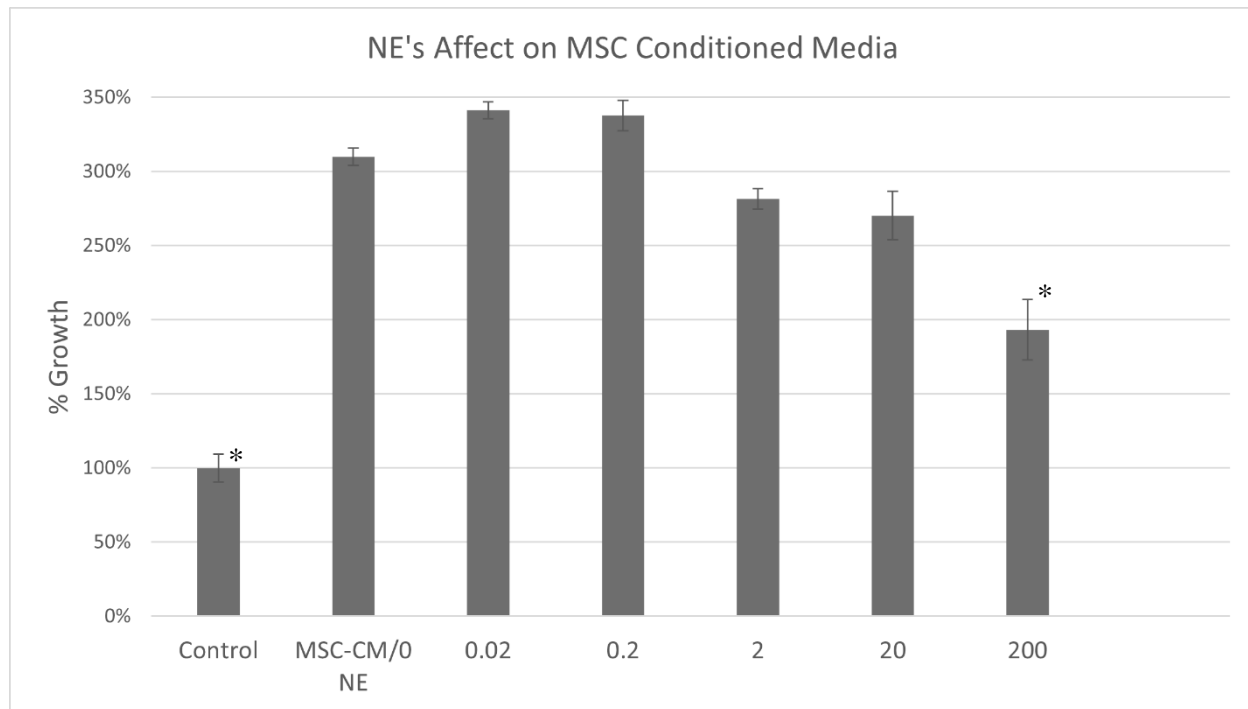


Figure 22. The Degradation of MSC Conditioned Products by Various Concentrations of NE. Elastase Concentrations: 200, 20, 2, 0.2, 0.02 mU/mL. *Statistical significant when compared to sample MSC-CM/0 NE, $p \leq 0.05$ and $F_{crit} \leq F$.

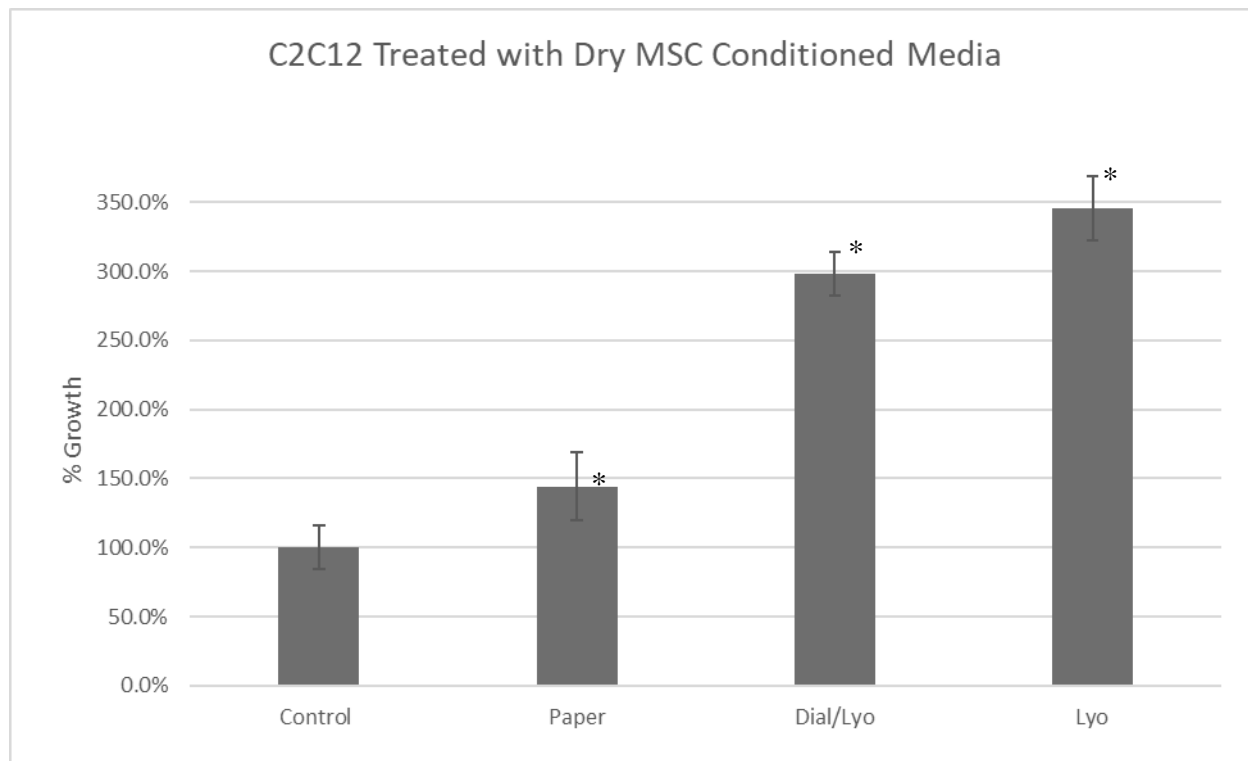


Figure 23. Um-MSC Conditioned Media in Various Treatment Forms Tested for Inducing Proliferation of C2C12 Cells. *Statistically significant with $p \leq 0.05$ and $F_{crit} \leq F$ when compared to the untreated control.

5.4 Statistical Analysis for the Proliferation Assays

From all proliferation experiments standard deviation from the average fluorescence from Hoechst assays for each sample was calculated, and % standard deviation was applied to each graphical representation of the data. Additionally, a single factor Anova ($p \leq 0.05$) was performed from the data for each experimental MSC-CM treatment group and compared to the control (Figure 21 & 23). For comparisons between MSC conditioned media groups to their respective untreated control the P-value was $p \leq 0.05$ with $F \geq F_{crit}$ for all MSC conditioned media treatments. For Figure 22 the single factor Anova was performed between the data from the differing concentrations of NE to the wells that received 0 mU/mL NE, where $p \leq 0.05$, $F \geq F_{crit}$.

Chapter 6: An Essential Combination of Protease Inhibition with the Delivery of a Um-MSc Conditioned Media

From in vitro investigation, and prior work by the author and laboratory^{13, 18}, it is observed as essential to protect any growth factor therapies for healing HtHWs through an accompanying treatment of protease inhibition. Growth factors have been a target therapy for healing chronic wounds^{7, 30, 31}, including the use of stem cell-based products³². However, it is observed that not much research has yet translated into mainstream use in clinical settings, while still today remaining a large topic in the conversation of healing wounds faster. Whether it be the limited efficacy of basic growth factor combinations strained by proteolytic degradation, or limited means of funding for translation, there exists a clear need for a therapy with high efficacy and that can be produced on a large scale at low costs while also minimizing wound care tasks for the clinician. All of these needs can be answered utilizing the right protein combinations to create a growth factor cocktail that is both highly potent and self-protecting to elevate the usefulness of the treatment.

In past work done by this author¹³ and laboratory¹⁸, the main focus was on creating recombinant proteins such as recombinant growth factors to be combined with recombinant protease inhibitors for inhibition. Despite ease in plasmid expression and purification, utilizing recombinant processes and ITC, there exists a need for a simpler and cost-effective way to produce a growth factor cocktail with all of the essential proteins. Here it is described that a combination of the dual protease inhibitor, and a um-MSc conditioned media containing growth factors can be protected and delivered to heal HtHWs.

6.1 The Proteolytic Degradation of Therapeutic Proteins

As previously described by the author¹³, a simple experiment was employed to observe the direct effect of proteolytic degradation of growth factors, in vitro, in the presence of proteases. A recombinant keratinocyte growth factor, rhKGF, was incubated in the presences of either NE or MMP2. NE and MMP 2 were added to samples with or without the dual protease inhibitor, PMPD2-L10Flag-APPIP. Each sample was incubated for 24-hours, including a control that just contained rhKGF. However, 2 hours and 4 hours after the start of the incubation a sample was taken from each experimental group. After the last samples are collected at the end of the 24-hour time point, a standard western blotting procedure was employed. An antibody specific to human KGF was used to stain the protein containing membrane and the resulting image captured using chemiluminescence.

6.1.1 The Protection of rhKGF from the Degradation Caused by NE and MMP2²

Figure 24 is the western blot observing the protection of rhKGF from proteolytic degradation using the dual protease inhibitor. Lane 1 is the biotinylated ladder, while lane two is a control sample of rhKGF. Lanes 3-4 show the degradation of rhKGF when no inhibitor is present. It is seen that in lanes 3 rhKGF is still present at the 2-hour mark while fully degraded in lanes 4 and 5, at the 4- and 24-hour time points respectively. When the protease is present, lanes 6-8, rhKGF remains present through all time points. In lanes 9-11, it is seen that rhKGF is almost fully degraded at the 24-hour mark by MMP2, while in lanes 12-14 the rhKGF is unaffected by MMP2 through all time points of the experiment. These results conclude that proteases indeed negatively influence locally residing growth factors, where in this experiment rhKGF was degraded quickly

² Information in Section 6.1 has previously been published in *Biotechnology Progress*. Strauss, G. & Koria, P. Hybrid fusion protein as a dual protease inhibitor for the healing of chronic wounds. *Biotechnology Progress* **37**, e3209 (2021). Permissions in Appendix B.

by NE, taking just 4 hours to destroy the rhKGF. Additionally, MMP2 had the same affect, but to a lesser degree. These results also show the importance of the dual protease inhibitor for the protection of rhKGF, where, when the dual inhibitor was present, the rhKGF remained for the entirety of the 24-hour experiment.

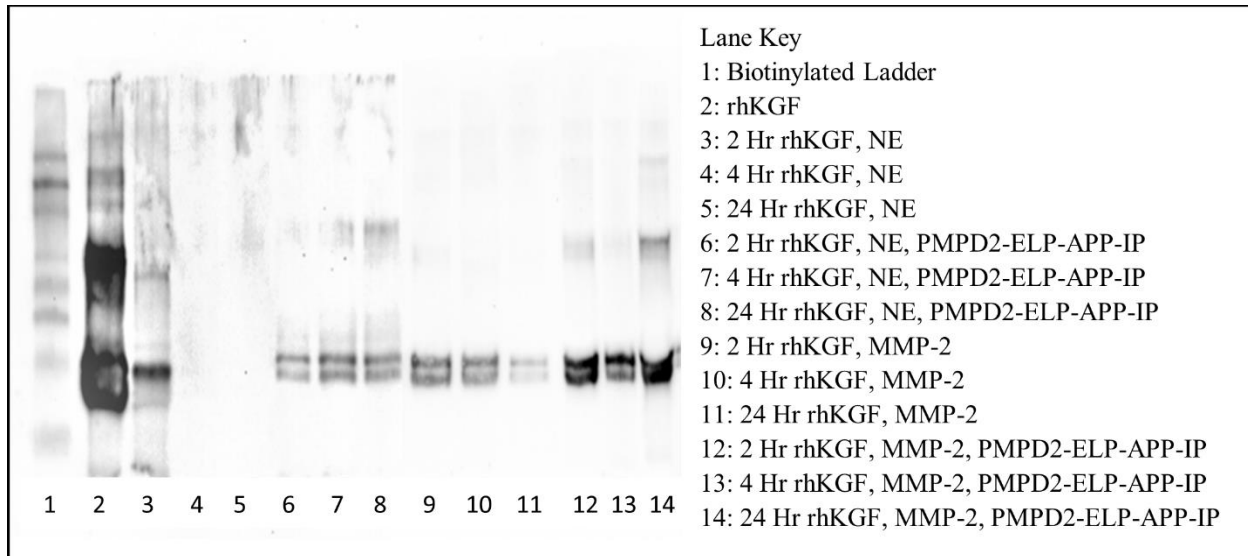


Figure 24. A Western Blott Analyzing the Protection from Degradation of RhKGF in the Presence of NE and MMP2 Over a 24-Hour Incubation.

6.2 A Chronic Wound Diabetic Mouse Model

A combination of um-MSC conditioned media and the dual protease inhibitor were tested for wound healing capabilities, *in vivo*, in a diabetic chronic wound mouse model. The necessity for this combination has been shown valuable *in vitro*, but it is imperative that this combination is tested in a real wound environment. The animal model protocol run here, followed regulatory, timeframe, and animal safety guidelines set out by the University of South Florida's Institutional Animal Care and Use Committee (IACUC) before, during, and after the animal experiment was employed and the approval can be viewed in Appendix B of this manuscript. Nine diabetic mice

were obtained from The Jackson Laboratory. All mice ordered and received from The Jackson Laboratory were female and of the strain 000697, a B6.BKS(D)-Lepr db/ that were 6-8 weeks old. Upon arrival the mice were left to acclimate for 7 days before a wounding procedure was employed. Fourteen days after the initial therapeutic treatments, the mice were euthanized, and tissue samples were collected from the wound of each mouse to evaluate whether reepithelization and matrix deposition occurred when treated with the combination of PMPD2-L10Flag-APPIP and um-MSD conditioned media.

6.2.1 A Surgical Wounding Procedure

After mice arrival and a 7-day acclimation period, the mice underwent the following wounding procedure. One mouse at a time was anesthetized utilizing isoflurane and shaved on the middle of the back of the mouse. Once shaved, if there was a large density of hair on the mouse, Nair was utilized to make the back of the mouse bald in the area of incision. It is important to get a clean shave to ensure a durable application of the bandages at the end of the wounding procedure. Once cleanly shaved and sterilized with an alcohol pad, a 1 cm x 1 cm square, scored with a permanent marker was applied. The incision was made utilizing 11.5 cm straight blade Metzenbaum scissors to cut along the scored 1 cm x 1 cm square on the skin of the mouse. The incision was started at a corner of the square by pulling up one corner with Graefe forceps and making the initial cut with the skin tuff pulled off the back of the mouse, and then cutting along the rest of the scoring lines. Once the 1 cm x 1 cm incision is made the resulting square piece of skin was removed from the back of the mouse.

6.2.2 NE Pretreatment for Modeling and Inducing a Chronic Wound Environment

Nine mice were pretreated with NE for 7 days to model a chronic wound environment before therapeutic treatments. Fractions of fibrinogen and thrombin were prepared to then mix to

become a fibrin gel for the delivery of both NE and the therapeutic treatments. The fibrinogen fraction was prepared by making a stock solution at a concentration of 62.5 mg/mL. The working fibrinogen solution is achieved by diluting the stock 1:10 in 1xPBS. While the thrombin working solution was made from the mixing of 50 μ l of 100 U/mL solution of thrombin, 5 μ l of 1 M CaCl₂, and 345 μ l of deionized H₂O. During wounding the thrombin fraction was placed on ice and the fibrinogen fraction was placed in a 37°C water bath. When ready to apply a fibrin gel to the wound on the back of the mouse, 20 μ l of the thrombin fraction is combine with 80 μ l of the fibrinogen fraction and mixed. NE was added to the fibrin gel to a final NE concentration in the 100 μ l gel of 250 mU/mL (a clinically relevant concentration in chronic wounds) and then applied to the wound and let to solidify for 2 minutes. The mouse was then bandaged, removed from the isoflurane, and observed until fully awake. This NE pretreatment for 9 mice was done twice in the 7-day pretreatment period and then therapeutic treatments were employed.

6.2.3 Treating the Mice Wounds with Fibrin Gels Containing the Dual Protease Inhibitor and Um- MSC Conditioned Media

Fibrin gel preparation here follows the procedure outlined in section 6.2.2, however PMPD2-L10Flag-APPIP is added to the fibrinogen fraction for 3 mice receiving a full treatment of both inhibitor and um-MSC conditioned media, with a final concentration of 1 μ g/ μ l. Um-MSC conditioned media was dialyzed, frozen, and lyophilized. The resulting powder was added into the fibrinogen fraction at a concentration of 0.5 μ g/ μ l, in accordance with the conditioned media volume that showed results in the *in vitro* proliferation studies. Before treatment the thrombin fraction was placed on ice, while the fibrinogen fraction containing um-MSC conditioned powder, and the dual protease inhibitor was placed in a 37°C bath. The fibrin gel was made by adding 20 μ l of the thrombin fraction to 80 μ l of the fibrinogen/inhibitor/conditioned media fraction. Then it

was lightly mixed and NE was added to the gel for a final concentration of 250 mU/mL. Next, the gel was added to the wound and let to solidify for 2 minutes. After the gel was solidified, bandages were applied, and the mouse was observed until awakening from the anesthesia.

Table 5. Treatment groups and controls for the chronic wound mouse model.

Treatment Groups	Format
Negative Control	7-Day NE Pretreatment + Continuous NE Treatment
MSC-CM Treated	7-Day NE Pretreatment + Continuous NE Treatment with Um-MSC Conditioned Powder
Full Treatment	7-Day NE Pretreatment + Continuous NE Treatment with Um-MSC Conditioned Powder and the Dual Protease Inhibitor

6.2.4 Tissue Collection and Histology

Fourteen days from the application of therapy, 21 days from NE pretreatment, the mice were euthanized, and wound tissue was collected. The mice were euthanized using a CO₂ flow rate of 10%-30% of cage volume per minute and a secondary means of euthanizing was employed via cervical dislocation. The wound tissues were collected after each mouse was euthanized, by cutting around the wound, leaving a halo of healthy tissue, with Metzenbaum scissors and pulling the entire circular wound off the back of each mouse. The wound was cut in half down the diameter of the tissue sample. Half of the wound was placed in a specimen mold with OCT compound with the wound edge placed down for tracking orientation for tissue sectioning. Immediately, the tissue sample in the cryomold was placed on dry ice for flash freezing, and then stored in -80°C until sectioning. The sectioning was performed by Moffit Cancer Center’s histology core. Tissue samples were sectioned to obtain a full tissue section of the cross section of the wound. Trichrome

stains were employed and analyzed in microscopy to evaluate the degree of healing through identifiable features such as re-epithelialization and collagen matrix formation in the wound samples.

6.3 Chronic Wound Mouse Model Results

Figure 25 shows representative images of 2 mice that were NE pretreated and was treated continuously with NE throughout the experiment but did not receive a therapeutic treatment. While Figure 26 displays mice that got pretreated and continuous treatment with NE, but at the start of therapeutic treatments received um- MSC conditioned media and continued therapeutic treatment throughout the experiment. Figure 27 displays mice that were pretreated and continuously treated with NE, however this mice group received a full therapeutic treatment of both um- MSC conditioned media and the dual inhibitor, PMPD2-L10Flag-APPIP.

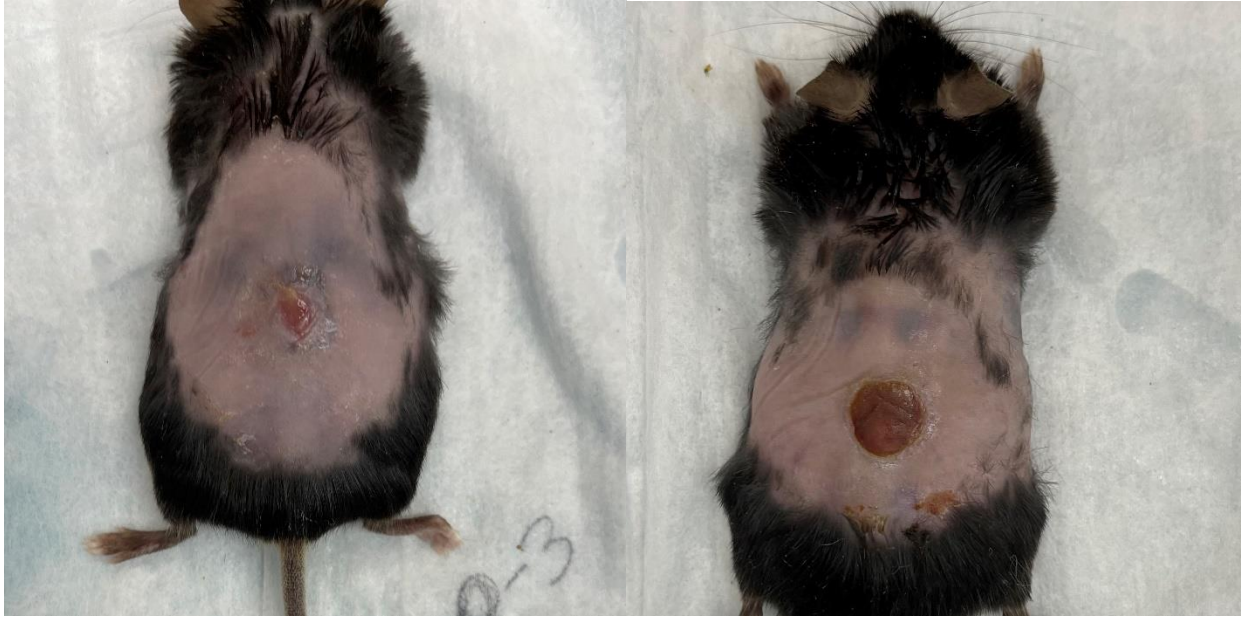


Figure 25. Representative Images of the Mice Wounds from the NE Pretreated Controls Taken at the Experiments End Point.

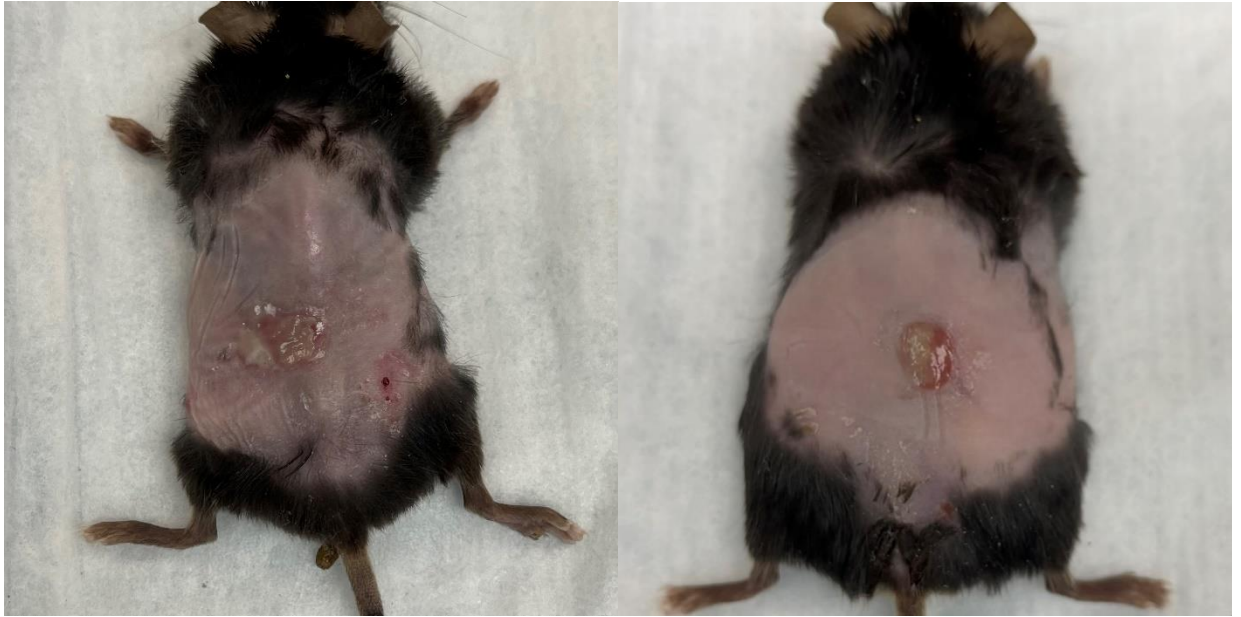


Figure 26. Representative Images of the Mice Wounds from the Experimental Groups that were NE Pretreated and then Received MSC Conditioned Media Treatments with Continuous NE Treatments.

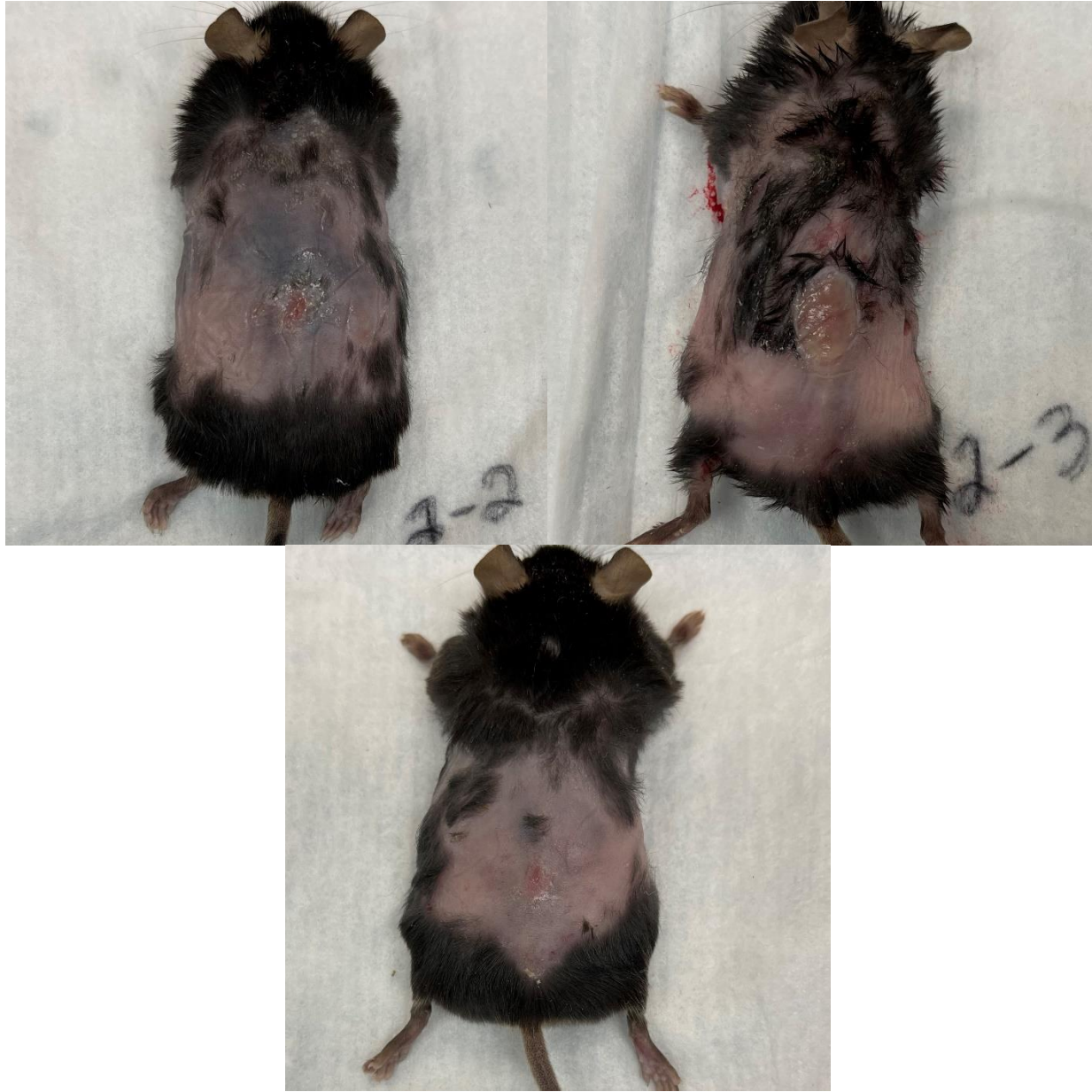


Figure 27. Representative Images of the Mice Wounds from the Experimental Groups that were NE Pretreated and then Received MSC Conditioned Media and PMPD2-L10Flag-APP with Continuous NE Treatments.

6.3.1 An Analysis of Wound Epidermal Thickness and Collagen Composition

Tissue sections were stained with a Masson's trichrome stain to evaluate the degree of collagen composition and epidermal thickness of the center of each wound. Figure 28 A-C are representative images of mice wound tissue sections that underwent trichrome staining and pictures captured at 40x magnification. A qualitative analysis of these images show, in Figure 28 A-C, stained blue collagen strands between cell nuclei appearing light blue to gray in color with the nuclei of cells staining a dark blue to purple in color. Figure 28 A-B are images of the untreated control mouse wound and a mouse wound that was treated with just MSC-CM, respectively. When comparing the images in Figure 28 A-B to Figure 28 C it is apparent that normal tissue anatomy with visible layers of the skin are apparent in image C where a full therapeutic treatment of MSC-CM and PMPD2-L10Flag-APPIP was delivered, while in A and B there is a less defined skin anatomy.

ImageJ was utilized on the 40x microscopy images of trichrome staining of each tissue section from each mouse group, a image from the center of the wound was taken at 40x magnification, the scale was set in ImageJ to align with that of the scale of the 40x images. The epidermis from each image was measured for thickness three separate times across the epidermis of the tissue section to analyze epidermal thickness. The results from the epidermal thickness analysis can be seen in Figure 29. A 2.8-fold greater epidermal thickness was observed in the full treatment group over that of the untreated control mice. Furthermore, a 1.4-fold greater epidermal thickness was observed in the full treatment group over that of the mice that were treated with just MSC-CM. This result suggests that mice that received the full treatment, MSC-CM and PMPD2-L10Flag-APPIP, healed to a greater degree than the untreated control mice and mice simply treated with MSC-CM.

Additionally, an ImageJ analysis of collagen composition of the trichrome stains further confirms the more developed healing in the full treatment group. Figure 30 displays the results of average collagen composition of all mice from each group (untreated, MSC-CM treated, and MSC-CM plus the dual inhibitor) and their collagen composition of the wound 14 days following therapeutic treatment. In Figure 30 it is observed that a 1.7-fold increase in collagen composition, was achieved over the untreated control, observed by the full treatment group. However, the mice group that only received MSC-CM displayed collagen composition in amounts like that of the untreated control mice. Development of more collagen in the mice group that were treated with both MSC-CM and the dual inhibitor further suggests that the untreated control mice and mice just treated with MSC-CM are farther behind in healing than that of the full treatment group.

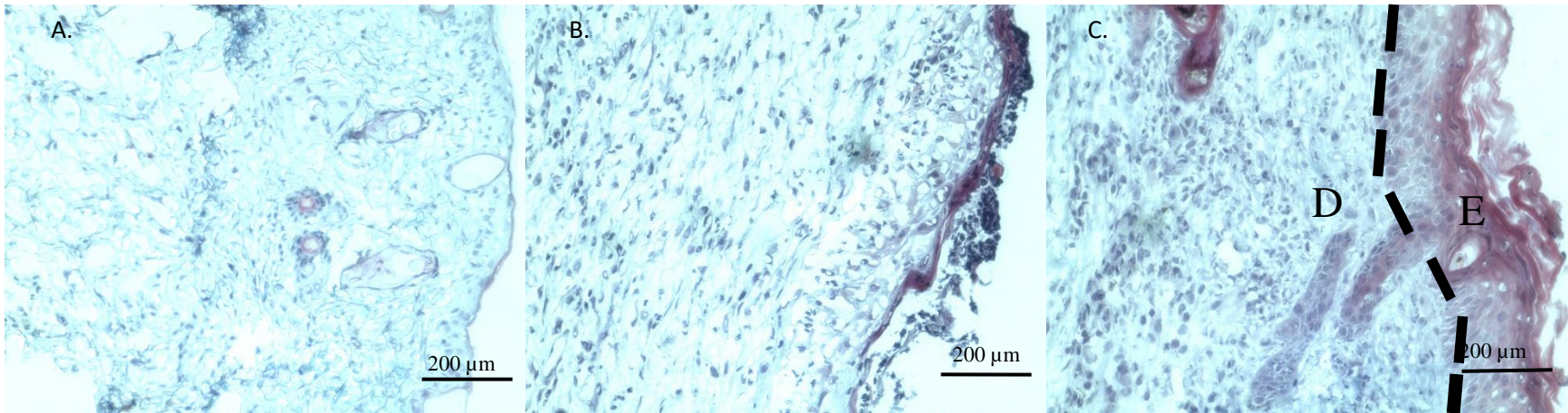


Figure 28. Representative Images of Masson's Trichrome Stained Wound Tissue Samples. Utilized for Collagen and Epidermal Thickness Quantifications Where A) is a Sample from the Untreated Control, B) is from the Treatment with MSC-CM, and C) Received the Full Treatment, MSC-CM and PMPD2-L10Flag-APPiP, Where the Dashed Line Represents the Basement Membrane, and E: Epidermis, D: Dermis

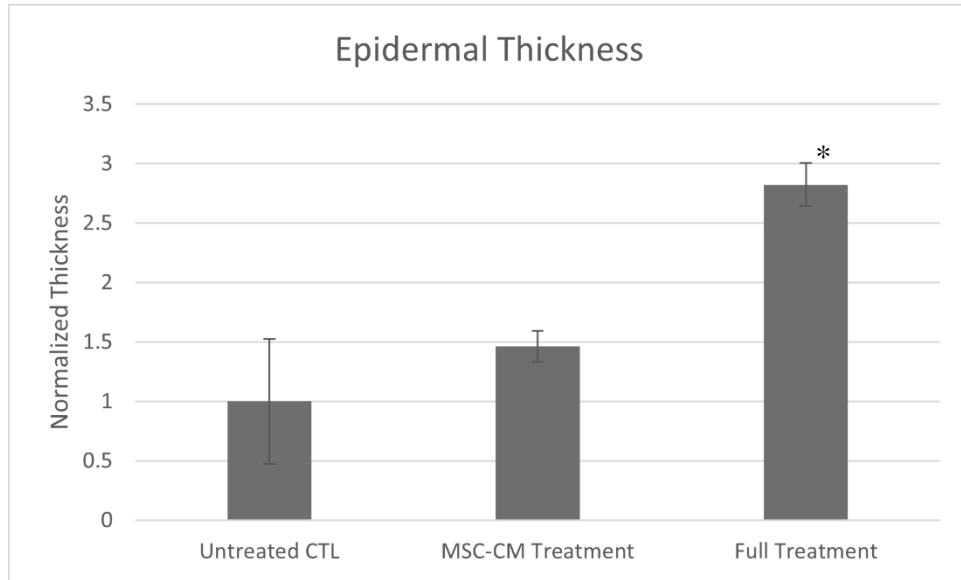


Figure 29. The Average Epidermal Thickness from Tissue Samples Collected from Each Mouse Group Measured in ImageJ and Normalized to the Untreated Control. *Statistically significant when compared to the untreated control group with $p \leq 0.05$ and $F_{crit} \leq F$.

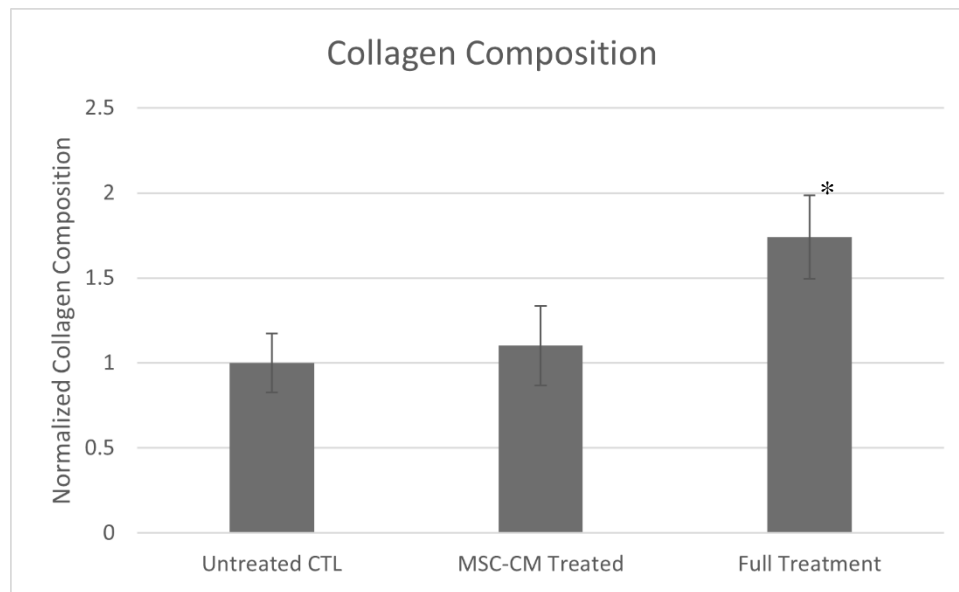


Figure 30. Collagen Composition of the Mice Wounds Normalized to the Collagen Composition of the Untreated Control. *Statistically significant with $p \leq 0.05$ and $F_{crit} \leq F$.

6.3.2 Statistical Analysis of Mouse Model Results

A single-factor Anova was ran between groups (Untreated, MSC-CM treated, MSC-CM and PMPD2-L10Flag-APPIP treated) for the ImageJ analysis of collagen composition. The difference of collagen composition between the Untreated controls and the mice treated with MSC-CM were statistically insignificant ($P \geq 0.05$, $F_{crit} \geq F$). This statistical result further confirms that there is no difference between mice in this experiment that go untreated and mice that just receive the treatment of MSC-CM and the null hypothesis cannot be rejected. In contrast, statistical significance was found when comparing mice that were treated with both MSC-CM and the dual inhibitor to mice that were untreated or treated with just MSC-CM. A single factor Anova was ran and P-values ≤ 0.05 were obtained with F-critical values less than the F-values. Meeting these two criteria alludes to significant differences between the full treatment group, and the mice that were untreated or treated MSC-CM.

Chapter 7: Discussion

Chronic wounds and wounds with delayed healing have been on the forefront of costly medical treatment for decades. Though delayed wound healing has traditionally affected those who belong to elderly populations, the impact chronic wounds have on the healthcare system is continually rising from an increase in prevalence of obesity related diseases in even middle-aged populations^{1,2}. Given the association between chronic wounds and other diseases, it takes a well-rounded healthcare approach to prevent delayed wound healing. An all-encompassing approach to prevention and elimination of disease in a patient that suffer from delayed healing is important, but it does not necessarily address the root cause as to why a wound won't heal. Immediately, current chronic wounds would benefit from a therapeutic approach that simply focuses on closing a wound through rebalancing tissue degradation and deposition, while focusing on preventing new chronic wound formation on a patient through the advocacy of lifestyle changes and an immediate pursuit of medical treatment when a patient with chronic wound history obtains a new wound.

Current treatments have focused on very important concepts like debridement to get rid of unviable tissues and established infections^{7,8}. Practices such as debridement are very basic but may be absolutely necessary to get back to a wound environment that is not overwhelmed with dead tissues. However, some wounds may be so entirely halted in a phase of degradation, treatment methods like debridement may not be effective at all for the interruption of this vicious cycle, while needing to be employed repeatedly to eventually obtain positive results. Furthermore, it is apparent through this research and related research^{13,18}, that protein based treatments, currently

employed, will not survive the harsh wound environment in the presence of proteolytic degradation without the use of protease inhibitors.

This dry, three-component, protein-based therapeutic for the treatment of hard-to-heal wounds contains the functionalities necessary for restoring the balance between tissue degradation and deposition while containing characteristics related to sustained delivery and control in the application site. An expansion of research related to this protein cocktail include testing for its efficacy for sustained release, its effectiveness in human wound healing, and further research into application styles that may provide this therapeutic with the ability to treat any wound in any environment. Additionally, regenerative medicine practices utilizing stem cell products have been a prominent talking point for healing wounds and highly damaged tissue through the application of allograft tissue. However, regenerative medicine products are underproved for their efficacy in relation to delivering functional cells to injured tissue. Furthermore, most stem cell derived wound healing products that contain live cells or solubilized proteins require unique and expensive storage conditions (-80°C and liquid nitrogen) and are therefore limited in shelf life, shipping constraints, and application styles. The benefit of a dry product is that it can be stored in ambient conditions and solubilized for delivery, applied dry directly in a wound, mounted in a gel for sustained release, embedded in materials, and even applied as a powder coating on a bulk material.

Growth factors are a part of the natural wound healing progression to cause cellular migration, proliferation, and growth^{30, 33}. Here it is seen that growth factors fall victim to proteases secreted in a wound whether that be growth factors in a therapeutic or ones that are secreted as a normal part of the wound healing cycle. This predicament has been displayed by other researchers as well^{12, 18, 34}. Therefore, any protein based therapeutic combination must protect itself, and healthy tissues, through the addition of protease inhibitors to accompany growth factors. With this

knowledge a thoughtful approach has been developed to yield this wound healing product that spikes proliferation while interrupting tissue and protein degradation. Utilizing the engineered dual protease inhibitor, PMPD2-L10Flag-APPIP, an all-encompassing protein cocktail harvested from UM-MSCs, and an engineered tethering protein, all as a therapeutic protein-based combination is valuable on both the level of therapeutic efficacy and economic practicality. Economically, protein synthesis can be very expensive due to the sheer number of proteins that would need to be synthesized and purified separately if a protein cocktail, like the um-MSC biproducts of conditioning media, were to be made recombinantly. However, the utilization of stem cells to condition media into a cocktail of growth factors and proteins is extremely cost effective and utilizing it as a therapeutic is merely considered an allograft approach. Additionally, cloning and recombinant technology utilized to create both PMPD2-L10Flag-APPIP and L10Flag-PIGF2 is a cost-effective approach especially when working off of a elastin-like peptide backbone where temperature alterations, pH changes, and centrifugation are the only driving forces to obtain a purified product.

Chapter 8: Key Developments

- A multi-target protease inhibitor was constructed as a single protein molecule with the ability to inhibit elastase and matrixmetalloproteinase-2, two proteases in elevated levels in chronic wounds and delayed wounds.
- The implementation of pI-Based Phase Separation during inverse transition cycling for the successful and cost-effective purification of dual ELP-fusion proteins.
- Protocols and processing procedures to harvest a potent growth factor cocktail that can be mixed with ELP-fusion proteins and freeze-dried into a dry powder.
- The combination of um-MSC conditioned media with the dual protease inhibitor, PMPD2-L10Flag-APPIP, to yield a protein combination that is self-protecting from proteolytic degradation in the wound site and protects healthy tissues that would otherwise be unnecessarily degraded by high levels of protease.
- The addition of a protein-based tethering system utilizing L10Flag-PIGF2 to further sustain the presence and diffusional control of the dual inhibitor beyond the limitations of aggregation caused by charge distribution and repulsive interactions between the bioactive ends of the dual inhibitor.
- The creation of a dry protein-based combination for the extension and ease of shelf life and storage, versatility of application style, and application in harsh environments (i.e. battlefields, underserved countries).

References

1. Sen, C.K. et al. Human skin wounds: a major and snowballing threat to public health and the economy. *Wound Repair Regen* **17**, 763-771 (2009).
2. Sen, C.K. Human Wounds and Its Burden: An Updated Compendium of Estimates. *Adv Wound Care (New Rochelle)* **8**, 39-48 (2019).
3. Davis, M.R., Gurtner, G.C. & Eriksson, E. Wound care research sponsored by the Department of Defense. *Wound Repair and Regeneration* **30**, 151-155 (2022).
4. Jarbrink, K. et al. Prevalence and incidence of chronic wounds and related complications: a protocol for a systematic review. *Syst Rev* **5**, 152 (2016).
5. Han, G. & Ceilley, R. Chronic Wound Healing: A Review of Current Management and Treatments. *Adv Ther* **34**, 599-610 (2017).
6. Sutcliffe, J. et al. Changes in the extracellular matrix surrounding human chronic wounds revealed by 2-photon imaging: second harmonic imaging of chronic wound extracellular matrix. *International Wound Journal* **14** (2017).
7. Demidova-Rice, T.N., Hamblin, M.R. & Herman, I.M. Acute and impaired wound healing: pathophysiology and current methods for drug delivery, part 1: normal and chronic wounds: biology, causes, and approaches to care. *Adv Skin Wound Care* **25**, 304-314 (2012).
8. Demidova-Rice, T.N., Hamblin, M.R. & Herman, I.M. Acute and Impaired Wound Healing: Pathophysiology and Current Methods for Drug Delivery, Part 2: Role of Growth Factors in Normal and Pathological Wound Healing: Therapeutic Potential and Methods of Delivery. *Adv Skin Wound Care* **25** (2012).
9. Razyieva, K. et al. Immunology of Acute and Chronic Wound Healing. *Biomolecules* **11**, 700 (2021).
10. Lindsay, S., Oates, A. & Bourdillon, K. The detrimental impact of extracellular bacterial proteases on wound healing. *International wound journal* **14**, 1237-1247 (2017).
11. Armstrong, D.G. & Jude, E.B. The role of matrix metalloproteinases in wound healing. *J Am Podiatr Med Assoc* **92**, 12-18 (2002).
12. McCarty, S.M. & Percival, S.L. Proteases and Delayed Wound Healing. *Adv Wound Care (New Rochelle)* **2**, 438-447 (2013).
13. Strauss, G. & Koria, P. Hybrid fusion protein as a dual protease inhibitor for the healing of chronic wounds. *Biotechnology Progress* **37**, e3209 (2021).
14. Ferreira, A.V. et al. Detection of human neutrophil elastase (HNE) on wound dressings as marker of inflammation. *Applied microbiology and biotechnology* **101**, 1443-1454 (2017).
15. Bergant Suhodolčan, A., Luzar, B. & Kecejl Leskovec, N. Matrix metalloproteinase (MMP)-1 and MMP-2, but not COX-2 serve as additional predictors for chronic venous ulcer healing. *Wound repair and regeneration* (2021).

16. Supuran, C.T., Scozzafava, A. & Mastrolorenzo, A. Bacterial proteases: current therapeutic use and future prospects for the development of new antibiotics. *Expert Opinion on Therapeutic Patents* **11**, 221-259 (2001).
17. Barrientos, S., Stojadinovic, O., Golinko, M.S., Brem, H. & Tomic-Canic, M. Growth factors and cytokines in wound healing. *Wound Repair Regen* **16**, 585-601 (2008).
18. Boeringer, T., Gould, L.J. & Korja, P. Protease-Resistant Growth Factor Formulations for the Healing of Chronic Wounds. *Advances in Wound Care (2162-1918)* **9**, 612 (2020).
19. Ndinguri, M.W., Bhowmick, M., Tokmina-Roszyk, D., Robichaud, T.K. & Fields, G.B. Peptide-based selective inhibitors of matrix metalloproteinase-mediated activities. *Molecules* **17**, 14230-14248 (2012).
20. Korja, P. et al. Self-assembling elastin-like peptides growth factor chimeric nanoparticles for the treatment of chronic wounds. *Proc Natl Acad Sci U S A* **108**, 1034-1039 (2011).
21. Mikaël, M.M. et al. Growth Factors Engineered for Super-Affinity to the Extracellular Matrix Enhance Tissue Healing. *Science* **343**, 885-888 (2014).
22. Pereira, T. et al. MSCs conditioned media and umbilical cord blood plasma metabolomics and composition. *PLoS One* **9**, e113769-e113769 (2014).
23. Berebichez-Fridman, R. et al. The Holy Grail of Orthopedic Surgery: Mesenchymal Stem Cells-Their Current Uses and Potential Applications. *Stem Cells Int* **2017**, 2638305-2638305 (2017).
24. Chen, W. et al. Angiogenic and osteogenic regeneration in rats via calcium phosphate scaffold and endothelial cell co-culture with human bone marrow mesenchymal stem cells (MSCs), human umbilical cord MSCs, human induced pluripotent stem cell-derived MSCs and human embryonic stem cell-derived MSCs. *J Tissue Eng Regen Med* **12**, 191-203 (2018).
25. Zhang, J. et al. Exosomes released from human induced pluripotent stem cells-derived MSCs facilitate cutaneous wound healing by promoting collagen synthesis and angiogenesis. *J Transl Med* **13**, 49 (2015).
26. Yu, Y. et al. Human fetal liver MSCs are more effective than adult bone marrow MSCs for their immunosuppressive, immunomodulatory, and Foxp3(+) T reg induction capacity. *Stem Cell Res Ther* **12**, 138 (2021).
27. Demidova-Rice, T.N., Wolf, L., Deckenback, J., Hamblin, M.R. & Herman, I.M. Human platelet-rich plasma- and extracellular matrix-derived peptides promote impaired cutaneous wound healing in vivo. *PLoS One* **7**, e32146 (2012).
28. Scott Schachtele, C.C., Joy Aho Markers and Methods to Verify Mesenchymal Stem Cell Identity, Potency, and Quality [White Paper]. *R&D Systems*.
29. Korja, P. Delivery of growth factors for tissue regeneration and wound healing. *BioDrugs : clinical immunotherapeutics, biopharmaceuticals and gene therapy*, 163 (2012).
30. Goldman, R. Growth factors and chronic wound healing: past, present, and future. *Adv Skin Wound Care* **17**, 24-35 (2004).
31. Park, J.W., Hwang, S.R. & Yoon, I.S. Advanced Growth Factor Delivery Systems in Wound Management and Skin Regeneration. *Molecules* **22** (2017).
32. Sharma, P., Kumar, A., Dey, A.D., Behl, T. & Chadha, S. Stem cells and growth factors-based delivery approaches for chronic wound repair and regeneration: A promise to heal from within. *Life Sci* **268**, 118932 (2021).
33. Steed, D.L. THE ROLE OF GROWTH FACTORS IN WOUND HEALING. *Surgical Clinics of North America* **77**, 575-586 (1997).

Appendix A: Abbreviation Key

- ELP: Elastin Like Peptide
- ITC: Inverse Transition Cycling
- pI: Isoelectric Point
- HtHW: Hard-to-Heal Wound
- MMP2: Matrix metalloproteinase-2
- MSC-CM: Mesenchymal Stem Cell Conditioned Media
- NE: Neutrophil Elastase
- pI-BPS: Isoelectric Point-Based Phase Separation
- Um-MSc: Umbilical Cord Derived Mesenchymal Stem Cells

Appendix B: Copyright Permissions

The permission below is for the use of material in Chapter 4 Sections 4.1-4.4, Section 2.2, and Section 6.1.

JOHN WILEY AND SONS LICENSE TERMS AND CONDITIONS

Jun 02, 2022

This Agreement between University of South Florida -- Graham Strauss ("You") and John Wiley and Sons ("John Wiley and Sons") consists of your license details and the terms and conditions provided by John Wiley and Sons and Copyright Clearance Center.

License Number	5314830421474
License date	May 23, 2022
Licensed Content Publisher	John Wiley and Sons
Licensed Content Publication	Biotechnology Progress
Licensed Content Title	Hybrid fusion protein as a dual protease inhibitor for the healing of chronic wounds
Licensed Content Author	Graham Strauss, Piyush Koria
Licensed Content Date	Sep 16, 2021
Licensed Content Volume	37
Licensed Content Issue	6
Licensed Content Pages	11
Type of Use	Dissertation/Thesis
Requestor type	Author of this Wiley article
Format	Print and electronic
Portion	Full article
Will you be translating?	No
Title	Protein-Based Therapeutic Combination for the Treatment of Hard-to-Heal Wounds
Institution name	University of South Florida
Expected presentation date	Jun 2022
Order reference number	05232022
Requestor Location	University of South Florida
	United States
	Attn: University of South Florida
Publisher Tax ID	EU826007151
Total	0.00 USD
Terms and Conditions	

Appendix C: IACUC Approval



RESEARCH INTEGRITY & COMPLIANCE
INSTITUTIONAL ANIMAL CARE & USE COMMITTEE

MEMORANDUM

TO: Piyush Korla,

FROM: Farah Moulvi, MSPH, IACUC Coordinator
Institutional Animal Care & Use Committee
Research Integrity & Compliance

DATE: 2/26/2021

PROJECT TITLE: Protease resistant growth factor nanoparticles for chronic wound healing

FUNDING SOURCE: USF department, institute, center, etc.

IACUC PROTOCOL #: R IS00008851

PROTOCOL STATUS: **APPROVED**

The Institutional Animal Care and Use Committee (IACUC) reviewed your application requesting the use of animals in research for the above-entitled study. The IACUC **APPROVED** your request to use the following animals in your **protocol for a one-year period beginning 2/26/2021:**

Mouse: B6: C57BL/6J (78 Weeks, either male or female))	120
Mouse: B6.BKS-Leprdb (6-8 Weeks either male or female)	120

Please take note of the following:

- **IACUC approval is granted for a one-year period at the end of which, an annual renewal form must be submitted for years two (2) and three (3) of the protocol through the eIACUC system.** After three years all continuing studies must be completely re-described in a new electronic application and submitted to IACUC for review.
- **All modifications to the IACUC-Approved Protocol must be approved by the IACUC prior to initiating the modification.** Modifications can be submitted to the IACUC for review and approval as an Amendment or Procedural Change through the eIACUC system. These changes must be within the scope of the original research hypothesis, involve the original species and justified in writing. Any change in the IACUC-approved protocol that does not meet the latter definition is considered a major protocol change and requires the submission of a new application.
- **All costs invoiced to a grant account must be allocable to the purpose of the grant.** Costs allocable to one protocol may not be shifted to another in order to meet deficiencies caused by overruns, or for other reasons convenience. Rotation of charges among protocols by month without establishing that the rotation schedule credibly reflects the relative benefit to each protocol is unacceptable.

INSTITUTIONAL ANIMAL CARE AND USE COMMITTEE
PHS No. A4100-01, AAALAC No. 000434, USDA No. 58-R-0015